NASA/TM–2016-104606 / Vol. 46

Technical Report Series on Global Modeling and Data Assimilation, Volume 46

Randal D. Koster, Editor

MERRA-2 Input Observations: Summary and Assessment

Will McCarty, Lawrence Coy, Ronald Gelaro, Albert Huang, Dagmar Merkova, Edmond B. Smith, Meta Sienkiewicz, and Krzysztof Wargan

National Aeronautics and
Space Administration

Goddard Space Flight Center
Greenbelt, Maryland 20771

October 2016

NASA STI Program ... in Profile

Since its founding, NASA has been dedicated to the advancement of aeronautics and space science. The NASA scientific and technical information (STI) program plays a key part in helping NASA maintain this important role.

The NASA STI program operates under the auspices of the Agency Chief Information Officer. It collects, organizes, provides for archiving, and disseminates NASA's STI. The NASA STI program provides access to the NASA Aeronautics and Space Database and its public interface, the NASA Technical Report Server, thus providing one of the largest collections of aeronautical and space science STI in the world. Results are published in both non-NASA channels and by NASA in the NASA STI Report Series, which includes the following report types:

- TECHNICAL PUBLICATION. Reports of completed research or a major significant phase of research that present the results of NASA Programs and include extensive data or theoretical analysis. Includes compilations of significant scientific and technical data and information deemed to be of continuing reference value. NASA counterpart of peer-reviewed formal professional papers but has less stringent limitations on manuscript length and extent of graphic presentations.
- TECHNICAL MEMORANDUM. Scientific and technical findings that are preliminary or of specialized interest, e.g., quick release reports, working papers, and bibliographies that contain minimal annotation. Does not contain extensive analysis.
- CONTRACTOR REPORT. Scientific and technical findings by NASA-sponsored contractors and grantees.
- CONFERENCE PUBLICATION. Collected papers from scientific and technical conferences, symposia, seminars, or other meetings sponsored or co-sponsored by NASA.
- SPECIAL PUBLICATION. Scientific, technical, or historical information from NASA programs, projects, and missions, often concerned with subjects having substantial public interest.
- TECHNICAL TRANSLATION. English-language translations of foreign scientific and technical material pertinent to NASA's mission.

Specialized services also include organizing and publishing research results, distributing specialized research announcements and feeds, providing help desk and personal search support, and enabling data exchange services. For more information about the NASA STI program, see the following:

- Access the NASA STI program home page at http://www.sti.nasa.gov
- E-mail your question via the Internet to help@sti.nasa.gov
- Fax your question to the NASA STI Help Desk at 443-757-5803
- Phone the NASA STI Help Desk at 443-757-5802
- Write to:

  NASA STI Help Desk
  NASA Center for AeroSpace Information
  7115 Standard Drive
  Hanover, MD 21076-1320

NASA/TM–2016-104606 / Vol. 46

Technical Report Series on Global Modeling and Data Assimilation, Volume 46

Randal D. Koster, Editor

MERRA-2 Input Observations: Summary and Assessment

Will McCarty
NASA's Goddard Space Flight Center, Greenbelt, MD

Lawrence Coy
Science Systems and Applications, Inc., Lanham, MD

Ronald Gelaro
NASA's Goddard Space Flight Center, Greenbelt, MD

Albert Huang
Science Systems and Applications, Inc., Lanham, MD

Dagmar Merkova
Science Systems and Applications, Inc., Lanham, MD

Edmond B. Smith
Science Systems and Applications, Inc., Lanham, MD

Meta Sienkiewicz
Science Systems and Applications, Inc., Lanham, MD

Krzysztof Wargan
Science Systems and Applications, Inc., Lanham, MD

National Aeronautics and
Space Administration

Goddard Space Flight Center
Greenbelt, Maryland 20771

October 2016

Level of Review: This material has been technically reviewed by technical management

Available from

NASA STI Program
Mail Stop 148'
NASA Langley Research Center
Hampton, VA 23681–2199

National Technical Information Service
5285 Port Royal Road
Springfield, VA 22161
703–605–6000

This document is available for downloaded from the NASA Technical Reports Server (NTRS).
https://ntrs.nasa.gov

Abstract

The Modern-Era Retrospective Analysis for Research and Applications, Version 2 (MERRA-2) is an atmospheric reanalysis, spanning 1980 through near-realtime, that uses state-of-the-art processing of observations from the continually evolving global observing system. The effectiveness of any reanalysis is a function not only of the input observations themselves, but also of how the observations are handled in the assimilation procedure. Relevant issues to consider include, but are not limited to, data selection, data preprocessing, quality control, bias correction procedures, and blacklisting. As the assimilation algorithm and earth system models are fundamentally fixed in a reanalysis, it is often a change in the character of the observations, and their feedbacks on the system, that cause changes in the character of the reanalysis. It is therefore important to provide documentation of the observing system so that its discontinuities and transitions can be readily linked to discontinuities seen in the gridded atmospheric fields of the reanalysis. With this in mind, this document provides an exhaustive list of the input observations, the context under which they are assimilated, and an initial assessment of selected core observations fundamental to the reanalysis.

Contents

List of Figures

List of Tables

1. Introduction

The purpose of a reanalysis is to reconsider the historical record of observations with a modern, static data assimilation system. Therefore, the input observations are of fundamental importance to any reanalysis, and the character of the analyzed fields are naturally related to the character of the underlying observations. Because the quality and quantity of the observations change over time, it is important to document these changes so that they can be readily cross-referenced to changes in the character of the three-dimensional gridded fields.

The Modern-Era Retrospective Analysis for Research and Applications, Version 2 (MERRA-2, Gelaro et al. 2016), which begins in January 1980 and continues as a near-real time climate analysis, is a successor to MERRA (Rienecker et al. 2011), incorporating new observations and advances in modeling and data assimilation. Along with the observations, the fundamental links between MERRA and MERRA-2 are the Gridpoint Statistical Interpolation (GSI, Wu et al. 2002; Kleist et al. 2009) analysis scheme and the GEOS-5 atmospheric model (Rienecker et al. 2008, Molod et al. 2015), although both have undergone substantial development since MERRA. The validation of the MERRA-2 geophysical fields can be found in Bosilovich et al. (2015), and other advances to the system have been described elsewhere (e.g. Reichle and Liu 2014, Molod et al. 2015, Buchard et al. 2016, Randles et al. 2016ab, Takacs et al. 2016).

This document focuses on the input meteorological observations for MERRA-2 and their character – specifically those that are input to the GSI. The data considered in this paper fall under one of two fundamental classifications: conventional and satellite-based. For this discussion, conventional observations are primarily direct observations of the wind or mass field; some remotely-sensed, ground-based datasets, however, are also included in this classification. Spaceborne observations are further considered in terms of mass and wind observations. Mass observations from space include satellite radiances and retrieved measurements of the temperature and moisture fields. Satellite observations of wind include derived retrievals of surface and upper-air wind.

Both the conventional and spaceborne observing systems underwent considerable evolution over the course of the MERRA-2 period. While the configuration of the model and data assimilation systems is static, the underlying observations are fundamentally dynamic. Whether it be the introduction of new observing types or changes in the counts of existing observations, discontinuities in gridded fields or observation feedbacks can and will result from changes in the observing system.

Finally, a fundamental motivation for MERRA-2 is the fact that the MERRA system is quickly reaching the point where the loss of certain observing platforms could be catastrophic to the quality of the reanalysis. The most recent satellite in MERRA is NOAA-18, which launched in May 2005. Observations from subsequent platforms, including NOAA-19, the Metop series and Suomi-NPP, as well as new observation types from NASA Aura and GPS radio occultation, are utilized in MERRA-2. The MERRA-2 system is notably robust in the most recent periods in terms of spaceborne observations.

2. Input Observations

The types and sources of the observations assimilated in MERRA-2 are summarized in Table 1, and Figure 1 shows a summary of the observation counts over the course of the reanalysis prior to 2015. This section categorizes and details the global observing system, as its growth with time is clearly illustrated in the figure. All but two of the observation classifications in Figure 1 are specific to spaceborne remote sensing, the exceptions being aircraft and conventional (i.e. non-aircraft) observations. Accordingly, spaceborne observations represent the majority of the global observing system, and the percentage of the global observing system that is measured from space increases from 62% in Jan 1980 to 88% in Dec 2014.

2.1 Conventional Observations

The underlying conventional observations are core to any reanalysis. For the purpose of this document, they are classified into three groups: surface, upper air, and aircraft. The number of assimilated observations from each of these classifications during the course of MERRA-2 is shown in Figure 2. MLS temperature retrieval counts are also shown and are discussed in Section 2.3.3.

Surface observations are generally the same as those used in MERRA. Included in this classification are observations from ships, buoys, and land surface (e.g. meteorological aviation reports, or METAR), as well as the bogus Australian 'paid observation' (PAOB) surface pressures. MERRA-2 does not assimilate any estimates of tropical cyclone central surface pressure. However, tropical cyclones detected in the model background fields are relocated using the position given in the NCEP *tcvitals* reports via the methodology presented in Liu et al. (2000).

Upper air observations are fundamental to the reanalysis and are shown in Figure 2. These measurements are separated into two groups: direct and remotely sensed. The direct observations include measurements from sondes and pilot weather balloons (PIBAL). The number of direct observations is relatively constant over time, increasing only slightly since the early periods. The remotely sensed observations consist of wind vectors derived from ground-based instrumentation, specifically vertical azimuth display (VAD) winds from NEXRAD/WSR-88D radars and wind vector measurements from wind profilers. The remotely sensed observations begin with the Christmas Island Wind Profiler on 8 Jan 1987. The observation counts increase noticeably with the introduction of NOAA Profiler Network observations on 13 May 1992. An additional jump occurs on 16 June 1997 with the addition of NEXRAD VAD winds.

Aircraft measurements are also shown in Figure 2. The first significant increase in aircraft observations occurs in 1997. After that, the observation counts continue to increase with time and eventually become the dominant source of conventional direct measurements of mass and wind. These observations, however, are known to have biases in observed temperature. MERRA-2 incorporates an in-line bias correction procedure for aircraft temperature observations, tracked by individual tail numbers. The procedure and its performance are discussed in section 3.2.

MERRA-2 Observations and Data Sources			
Data Source/Type	**Period**	**Data Supplier**	**Classification**
Conventional Observations			
RAOB/PIBAL/Dropsonde	1 Jan 1980 - present	see Rienecker et al (2011)	Figure 2, Upper-Air (Direct)
AIREP/PIREP/ASDAR/MDCRS aircraft reports	1 Jan 1980 - present	NCEP, ECMWF	Figure 2, Aircraft
PAOB	1 Jan 1980 - 17 Aug 2010	NCEP, ECMWF, JMA, BOM	Figure 2, Surface
Surface land observations	1 Jan 1980 - present	NCEP	Figure 2, Surface
Surface ship and buoy observations	1 Jan 1980 - present	ICOADS	Figure 2, Surface
Ground-Based, Remotely Sensed Observations			
Wind profilers	14 May 1992 - present	UCAR, NCEP	Figure 2, Upper-Air (Remotely Sensed)
NEXRAD Vertical Azimuth Display Winds	16 June 1997 - present	NCEP	Figure 2, Upper-Air (Remotely Sensed)
Satellite-Derived Winds			
JMA Atmospheric Motion Vectors	1 Jan 1980 - present	NCEP, JMA	Figure 3, JMA
EUMETSAT Atmospheric Motion Vectors	1 Jan 1980 - present	NCEP, EUMETSAT	Figure 3, EUMETSAT
NOAA GOES Atmospheric Motion Vectors	1 Jan 1980 - present	NCEP	Figure 3, NOAA
NOAA/EUMETSAT AVHRR Atmospheric Motion Vectors	1 Oct 1982 - present	CIMSS	Figure 3, NOAA/EUMETSAT AVHRR
NASA EOS MODIS winds	1 Jul 2002 - present	CIMSS, NCEP	Figure 3, NASA MODIS
SSM/I & SSMIS Wind Speed (Version 7)	9 Jul 1987 - 29 Oct 2013	RSS	Figure 4, SSMI Wind Speed
QuikSCAT surface winds	19 Jul 1999 - 22 Nov 2009	JPL	Figure 4, QuikSCAT
ERS-1 surface winds	5 Aug 1991 - 21 May 1996	ESA	Figure 4, ERS/ERS-2
ERS-2 surface winds	19 Mar 1996 - 29 Mar 2011	ESA	Figure 4, ERS/ERS-2
ASCAT surface winds	15 Sep 2008 - present	NCEP	Figure 4, ASCAT
Satellite-Retrieved Measurements			
MLS Retrieved Temperature (Version 3.3)	13 Aug 2004 - 31 May 2015	NASA/GES DISC	Figure 2, MLS Retrieved T
MLS Retrieved Temperature (version 4.2)	1 June 2015 - Present	NASA/GES DISC	Figure 2, MLS Retrieved T
SSM/I rain rate	9 Jul 1987 - 16 Sept 2009	NASA/GES DISC	Figure 1, Precip
TMI rain rate	1 Jan 1998 - 8 Apr 2015	NASA/GES DISC	Figure 1, Precip
SBUV & SBUV/2 Ozone Retrievals (Version 8.6)	1 Jan 1980 - 31 Sept 2004	NASA/GES DISC	Figure 1, Ozone
MLS Retrieved Ozone (Version 2.2, ref)	1 Oct 2004 - 31 May 2015	NASA/GES DISC	Figure 1, Ozone
MLS Retrieved Ozone (Version 4.2, ref)	1 June 2015 - present	NASA/GES DISC	Figure 1, Ozone
OMI Retrieved Total Column Ozone (Version 8.5)	1 Oct 2004 - present	NASA/GES DISC	Figure 1, Ozone
Radio Occultation			
GPS/GNSS Bending Angle	15 July 2004 - present	NCAR, NCEP	Figure 1, GPSRO

Satellite Radiances			
Tiros-N Operational Vertical Sounder (MSU, SSU, HIRS-2)	1 Jan 1980 - 10 Oct 2006	NCAR, NESDIS	Figure 1, Heritage IR, MW
Advanced TOVS Infrared (HIRS-3, HIRS-4)	21 Jul 1998 - 16 Nov 2015	NESDIS	Figure 1, Heritage IR
Advanced TOVS Microwave (AMSU-A, AMSU-B, MHS)	1 Nov 1998 - present	NESDIS	Figure 1, Advanced MW
NASA EOS AMSU-A	1 Sept 2002 - present	NASA/GES DISC	Figure 1, Advanced MW
Advanced Technology Microwave Sounder	16 Nov 2011 - present	NESDIS	Figure 1, Advanced MW
Special Sensor Microwave Imager	9 Jul 1987 - 4 Nov 2009	RSS	Figure 1, SSMI
Atmospheric Infrared Sounder	1 Sept 2002 - present	NASA/GES DISC	Figure 1, AIRS
Infrared Atmospheric Sounding Interferometer	17 Sept 2008 - present	NESDIS	Figure 1, IASI
Cross-Track Infrared Sounder	7 Apr 2012 - present	NESDIS	Figure 1, CrIS
Geostationary Operational Environmental Satellite Sounder	24 April 2001 - present	NESDIS	Figure 1, Geo IR
Spinning Enhanced Visible and InfraRed Imager	15 Feb 2012 - present	NESDIS	Figure 1, Geo IR

Table 1 - The observations used, the temporal range, and the data suppliers of each conventional and remotely sensed observation type in MERRA-2. Each type includes a reference to the figure in this document that illustrates its assimilated observation count.

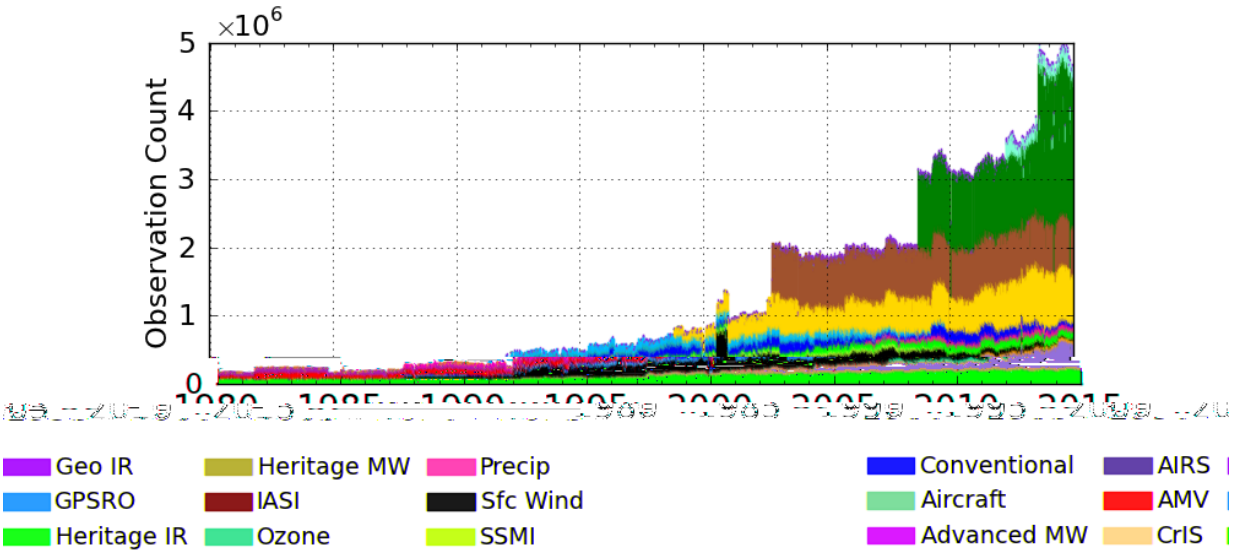

Figure 1 - Time series of assimilated observations for MERRA-2 for 1 January 1980 – 31 December 2014

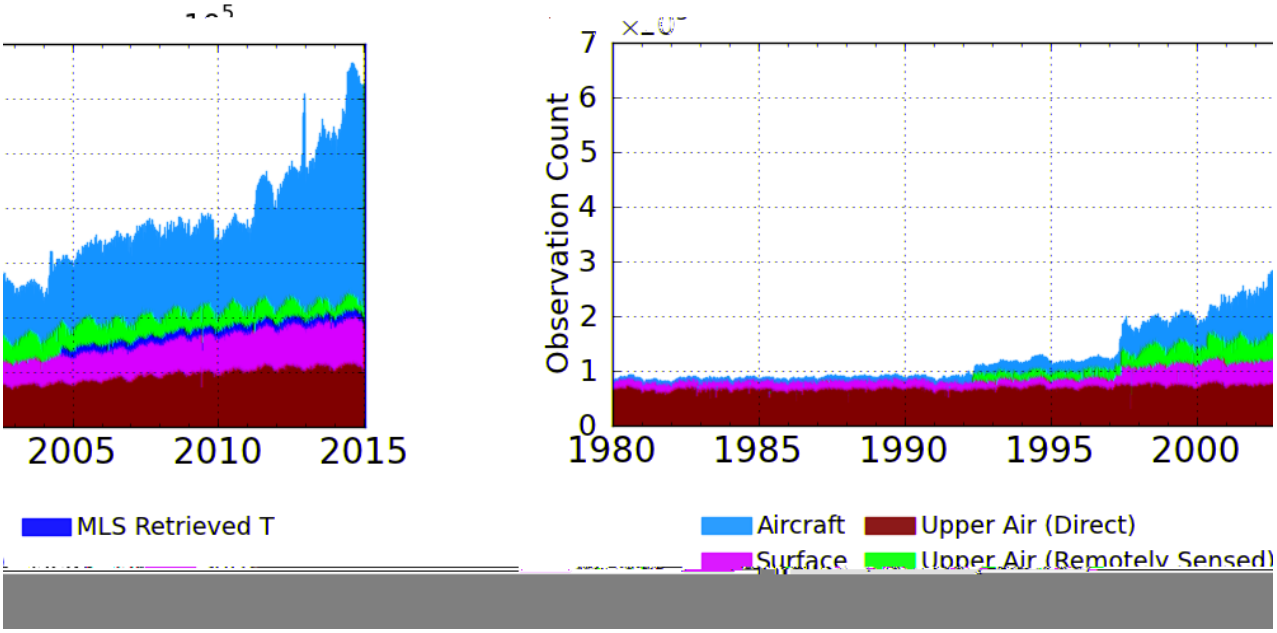

Figure 2 - Time series of input conventional observations for 1 January 1980 – 31 December 2014. Aircraft corresponds to the group of the same name in Figure 1, while all other observations are represented in the group "Conventional" in Figure 1.

2.2 Satellite Observations of Wind

Wind measurements derived from spaceborne platforms are used routinely throughout MERRA-2. The most common satellite-derived winds are atmospheric motion vectors (AMVs), which infer the wind by tracking features, specifically clouds and water vapor, from temporally successive satellite images. Time series of the AMV observation counts are shown in Figure 3. AMVs from imagers onboard geostationary satellites operated by the Japanese Meteorological Agency (JMA), European Organisation for the Exploitation of Meteorological Satellites (EUMETSAT), and the National Oceanic and Atmospheric Administration (NOAA) provide coverage over the midlatitudes and tropics. Specifically, those classified as JMA (Fig. 3) are derived from the Geostationary Meteorological Satellite (GMS), Multifunction Transport Satellite (MTSAT), and Himawari platforms. Those classified as EUMETSAT (Fig. 3) are derived from the Meteosat platforms. Those classified as NOAA (Fig. 3) are derived from the Geostationary Operational Evnironmental Satellite (GOES) platforms. AMVs from polar-orbiting platforms provide complementary coverage over the Arctic and Antarctic. The first classification of polar-orbiting AMVs is derived from the Advanced Very-High-Resolution Radiometer (AVHRR) imagers onboard the NOAA Polar Operational Environmental Satellites (POES) and EUMETSAT Meteorological Operational (MetOp) satellites (Fig. 3, NOAA/EUMETSAT AVHRR). The second classification of polar-orbiting AMVs is derived from the MODerate-resolution Imaging Spectroradiometer (MODIS) imagers onboard the NASA Terra and Aqua satellites (Fig. 3, NASA MODIS).

Geostationary AMVs are assimilated over the entire reanalysis, though early in the time series the counts are so small that they are difficult to see in Figure 3. The first polar AMV observations begin on 1 Oct 1982 with AVHRR (Dworak and Key 2009), which tracked clouds in the infrared window. A noted increase in NOAA geostationary observations occurs on 11 Mar 1998[1], as observations derived from the fully-automated processing for GOES AMVs described in Nieman et al. (1997) enter the reanalysis. This data stream is also the first to include water vapor winds (Velden et al. 1997). Beginning on 1 Jul 2002, MODIS AMVs (Key et al. 2003), which are derived from tracking both clouds and water vapor over the polar regions, are assimilated into the system. On 1 July 2010, AMV observations switched from being assimilated via the 'prep' preprocessor to being assimilated directly in the GSI. This increased the spatial density of the observations considered for assimilation. It is also noted that the polar AMVs are assimilated over the entire six-hour assimilation window, while the geostationary-derived AMVs are only considered during the hour prior to the center of the assimilation window.

In addition to AMVs, surface wind vectors and speeds derived from spaceborne instruments are assimilated into MERRA-2; the assimilated observation counts are shown in Figure 4. Surface wind vectors derived from scatterometry are available from European Space Agency (ESA) European Remote Sensing (ERS) and ERS-2 scatterometers, NASA Quick Scatterometer (QuikSCAT), and EUMETSAT Advanced Scatterometer (ASCAT). Surface wind vectors derived via polarmetric radiometry from the joint-NASA/NOAA/United States Department of Defense (DOD) WINDSAT instrument onboard the Coriolis satellite are also assimilated. Finally, surface

[1] GOES AMVs were inadvertently omitted in the reanalysis between 11 Jan 1996 and 10 Mar 1996

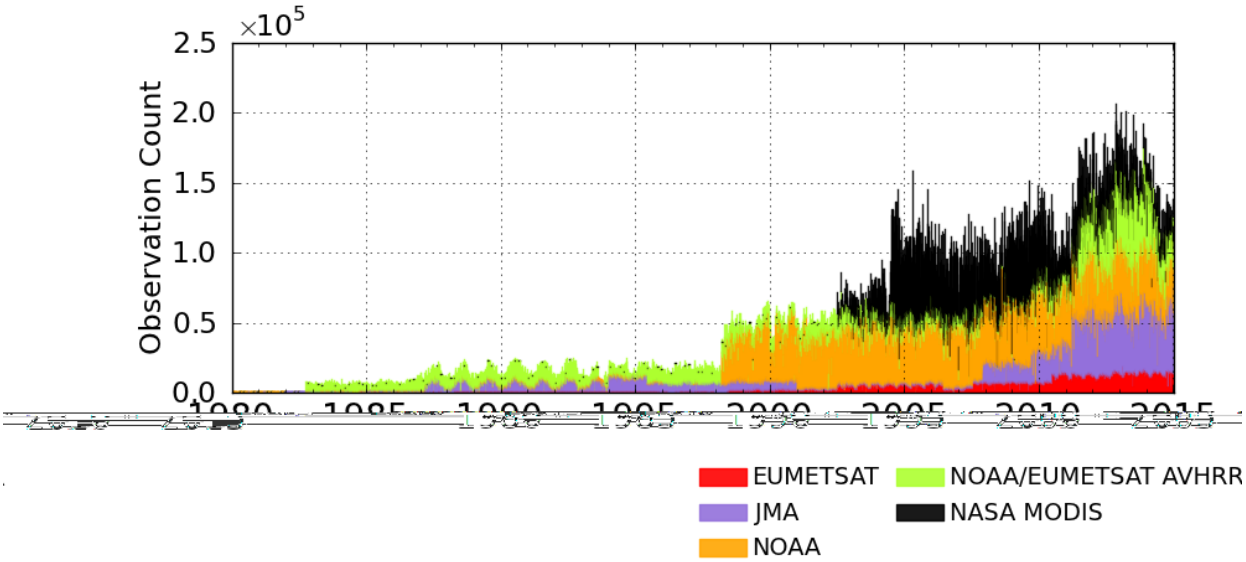

Figure 3 - Time series of input atmospheric motion vectors for 1 January 1980 – 31 December 2014. These observations are included in the "AMV" group in Figure 1.

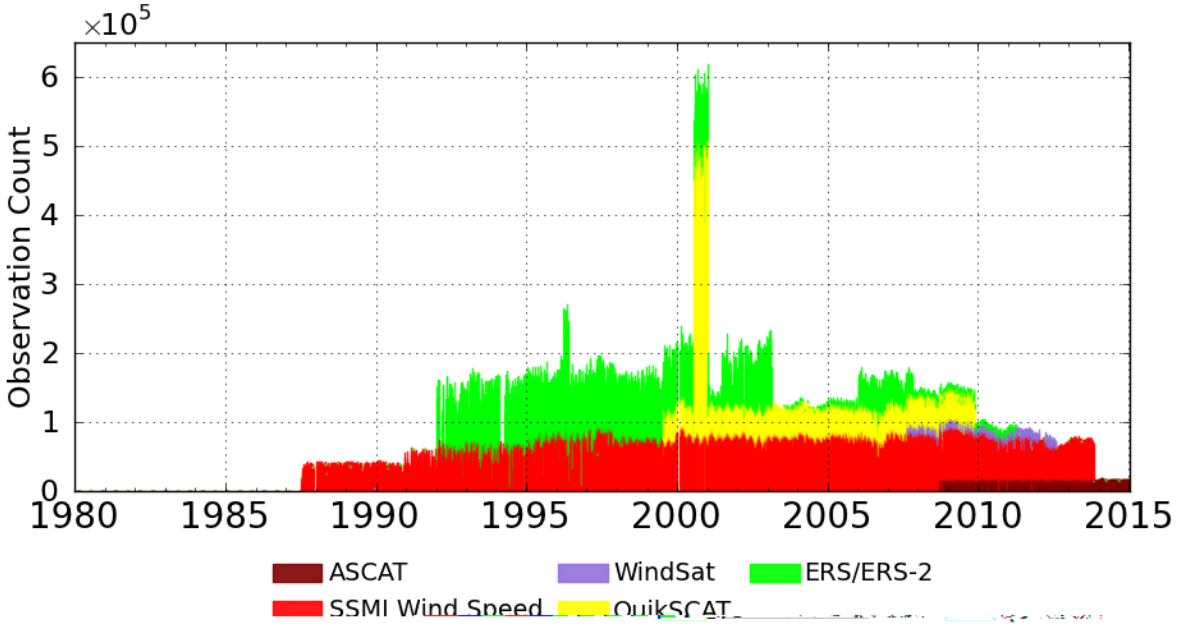

Figure 4 - Time series of input retrieved surface winds for 1 January 1980 – 31 December 2014. All observations are surface wind vectors except for the SSMI wind speed retrievals. These observations are included in the "Sfc Winds" group in Figure 1.

wind speed retrievals (Remote Sensing System Version 7, Wentz 2013) derived from Special Sensor Microwave Imager (SSM/I) and Special Sensor Microwave Imager/Sounder (SSMIS) microwave imagers on the United States Defense Meteorological Satellite Program (DMSP) platforms are also used in MERRA-2.

Figure 4 shows a dramatic but relatively short-lived increase in the number of QuikSCAT observations between 19 July and 31 December 2000. This corresponds to an error in preprocessing where observations beyond the mid-swath *sweet spot* were accepted into the analysis. This increase is also visible in the increase of surface wind observations in Figure 1. The count of ERS-2 observations dropped dramatically after 22 June 2003, when the onboard data storage on the platform failed and only those observations that could be downlinked in real time from the satellite were obtained.

2.3 Satellite Observations of Mass

2.3.1 Satellite Radiances

The vast majority of global temperature and moisture information is determined from the direct assimilation of satellite radiances. These observations fall into 5 categories:

- Microwave Temperature Sounders (MSU, AMSU-A, ATMS)
- Microwave Humidity Sounders (AMSU-B, MHS, ATMS)
- Microwave Imagers (SSM/I)
- Polar-Orbiting Infrared Sounders (SSU, HIRS/2, HIRS/3, HIRS/4, AIRS, IASI, CrIS)
- Geostationary Infrared Imagers and Sounders (GOES Sounder, SEVIRI)

A timeline for the platforms on which these instruments were flown is given in Figure 5 and Table 2. The core observations are the Tiros-N Operational Vertical Sounder (TOVS) and Advanced TOVS (ATOVS) suites. The TOVS instruments, which were flown on Tiros-N and NOAA-5 through NOAA-14, consisted of the Microwave Sounding Unit (MSU), the Stratospheric Sounding Unit (SSU), and High Resolution Infrared Radiation Sounder/2 (HIRS/2) instruments. The ATOVS era, which began with NOAA-15 and continues through Metop-B, replaced the MSU and SSU instruments with the Advanced Microwave Sounding Unit-A (AMSU-A). Microwave humidity radiance measurements were added to the ATOVS suite first with the Advanced Microwave Sounding Unit-B (AMSU-B) and later the Microwave Humidity Sounder (MHS) instruments. The HIRS/2 instrument was replaced with the HIRS/3 and later HIRS/4 instruments. More recently, the HIRS instruments have been replaced by hyperspectral infrared sounders, specifically the Atmospheric Infrared Sounder (AIRS), Cross-track Infrared Sounder (CrIS), and Infrared Atmospheric Sounding Interferometer (IASI). The AMSU-A and MHS instruments have been replaced by the Advanced Technology Microwave Sounder (ATMS) on the Suomi National Polar-orbiting Partnership (SNPP) and the upcoming Joint Polar Satellite System (JPSS) satellites.

In addition to sounder radiances, microwave imager radiances from SSM/I are assimilated. Specifically, version 7 of recalibrated SSM/I radiances from Remote Sensing System (RSS v7, Wentz 2013) are used. Prior to AMSU-B, this is the primary source of column water vapor

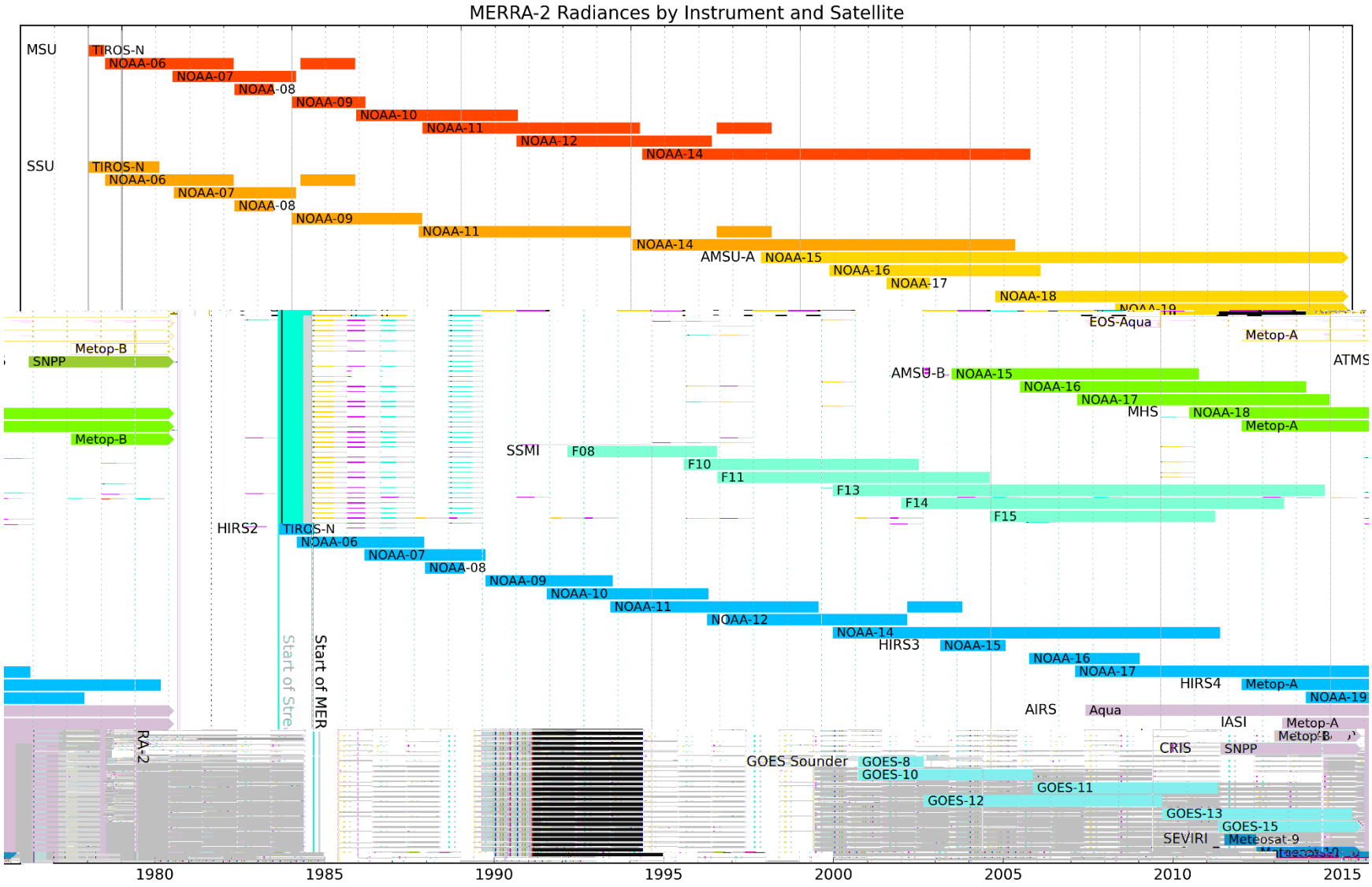

Figure 5 - Timeline of satellite radiance observations over the entire MERRA-2 period. Each bar is colored by instrument type and represents a satellite from which the instrument measured.

Satellite Radiances				
Platform	**Period**		**Platform**	**Period**
MSU			*SSM/I*	
NOAA-06	01 Jan 1980 - 17 Apr 1983		F08	10 Jul 1987 - 04 Dec 1991
	08 Apr 1985 - 17 Nov 1986		F10	09 Dec 1990 - 13 Nov 1997
NOAA-07	28 Jun 1981 - 18 Feb 1985		F11	05 Dec 1991 - 18 Dec 1999
NOAA-08	26 Apr 1983 - 20 Jun 1984		F13	03 May 1995 - 04 Nov 2009
NOAA-09	01 Jan 1985 - 07 Mar 1987		F14	08 May 1997 - 23 Aug 2008
NOAA-10	25 Nov 1986 - 01 Sep 1991		F15	18 Dec 1999 - 14 Aug 2006
NOAA-11	08 Nov 1988 - 10 Apr 1995		*HIRS-2*	
	15 Jul 1997 - 25 Feb 1999		TIROS-N	01 Jan 1980 - 20 Jan 1980
NOAA-12	18 Aug 1991 - 23 May 1997		NOAA-06	01 Jan 1980 - 17 Apr 1983
NOAA-14	01 May 1995 - 10 Oct 2006		NOAA-07	11 Jul 1981 - 04 Feb 1985
SSU			NOAA-08	26 Apr 1983 - 20 Jun 1984
TIROS-N	01 Jan 1980 - 04 Feb 1981		NOAA-09	03 Feb 1985 - 07 Nov 1988
NOAA-06	02 Jul 1979 - 17 Apr 1983		NOAA-10	25 Nov 1986 - 01 Sep 1991
	08 Apr 1985 - 17 Nov 1986		NOAA-11	12 Oct 1988 - 04 Dec 1994
NOAA-07	11 Jul 1981 - 18 Feb 1985			15 Jul 1997 - 28 Feb 1999
NOAA-08	26 Apr 1983 - 20 Jun 1984		NOAA-12	18 Aug 1991 - 14 Jul 1997
NOAA-09	01 Jan 1985 - 07 Nov 1988		NOAA-14	01 May 1995 - 30 Sep 2006
NOAA-11	28 Sep 1988 - 31 Dec 1994		*HIRS-3*	
	15 Jul 1997 - 25 Feb 1999		NOAA-15	02 Jul 1998 - 06 Jun 2000
NOAA-14	19 Jan 1995 - 04 May 2006		NOAA-16	16 Feb 2001 - 20 May 2004
AMSU-A			NOAA-17	25 Jun 2002 - 03 Dec 2011
NOAA-15	01 Nov 1998 - present		*HIRS-4*	
NOAA-16	05 Nov 2000 - 29 Jan 2007		NOAA-19	14 Apr 2009 - 05 Jul 2013
NOAA-17	15 Jul 2002 - 27 Oct 2003		Metop-A	21 May 2007 - 16 Nov 2015
NOAA-18	01 Oct 2005 - present		*AIRS*	
NOAA-19	14 Apr 2009 - present		Aqua	12 Oct 2002 - present
Metop-A	21 May 2007 - present		*IASI*	
Metop-B	13 Feb 2013 - present		Metop-A	01 Aug 2008 - present
Aqua	12 Oct 2002 - present		Metop-B	13 Feb 2013 - present
ATMS			*CrIS*	
Suomi NPP	16 Nov 2011 - present		Suomi NPP	01 Jan 2012 - present
AMSU-B			*GOES Sounder*	
NOAA-15	01 Nov 1998 - 16 Feb 2006		GOES 8	13 Apr 1994 - 01 Apr 2003
NOAA-16	05 Nov 2000 - 16 Apr 2009		GOES 10	25 Apr 1997 - 21 Jun 2006
NOAA-17	15 Jul 2002 - 22 Dec 2009		GOES 11	22 Jun 2006 - 05 Dec 2011
MHS			GOES 12	02 Apr 2003 - 13 Apr 2010
NOAA-18	01 Nov 2005 - present		GOES 13	15 Apr 2010 - 20 Nov 2015
Metop-A	21 May 2007 - present		GOES 15	07 Dec 2011 - present
Metop-B	13 Feb 2013 - present		*SEVIRI*	
			Meteosat 9	13 Feb 2012 - 21 Jan 2013
			Meteosat 10	21 Jan 2013 - present

Table 2 - List of start and end dates for satellite radiance measurement type, by instrument and platform, used in MERRA-2.

information globally, as HIRS water vapor channels provide limited information due to their sensitivity to clouds and resulting high rejection rates via quality control procedures.

Radiative transfer calculations necessary for the assimilation of satellite radiances are performed using the Community Radiative Transfer Model (CRTM, Han et al. 2006, Chen et al. 2008). The CRTM has been developed as a fast and accurate radiative transfer algorithm. The CRTM performs forward radiative transfer calculations of brightness temperature from input profiles of temperature, moisture, and ozone. Additionally, the CRTM calculates the Jacobians of brightness temperature with respect to the input profiles. The Jacobians are for the inversion of these radiances within the GSI analysis system. Monthly averaged profiles of carbon dioxide (Yang et al. 2012) are also incorporated into the CRTM calculations to account for the increase in CO_2 during the course of MERRA-2, although it is noted that CO_2 is not an analyzed variable in the reanalysis. The CRTM transmittance model used in MERRA-2 is the optical depth in pressure space (ODPS, Chen et al. 2012). Note also that for SSU, the CRTM incorporates a cell pressure correction as described in Chen et al. (2011).

Essential to the radiative transfer calculations is the definition of surface emissivity. For the infrared, surface emissivity over water is defined using the model of Nalli et al. (2008a,b), while the emissivity over all non-water surface types uses the database developed for the National Polar-orbiting Operational Environmental Satellite System (NPOESS) as described in the Han et al. (2006). For the microwave, the fast microwave ocean surface emissivity model, version 5 (FASTEM-5, Liu et al. 2011, Borman et al. 2012) is used over water, and the physical models described in Han et al. (2006) are used over the non-water surfaces.

Satellite radiances, unless explicitly stated otherwise in this section, are assimilated with a two-step bias correction procedure. First, a variational bias correction (Derber and Wu 1998) is applied to each channel of each instrument on each platform. This correction consists of five terms, which are a function of:

- the channel global mean background departure – the constant correction
- the cosine of the viewing zenith angle (for nadir-sounding instruments only),
- the retrieved cloud liquid water (for microwave instruments only),
- the lapse rate of the atmosphere scaled by the channel's weighting function – the first air mass correction term,
- and the square of the aforementioned scaled lapse rate – the second air mass term.

These terms are all scaled by variable coefficients that are updated as control variables as part of the GSI solution. At each datum, each bias estimate is determined as the product of each term and the corresponding coefficient. The sum of all these bias estimates is removed from the observation departures. These coefficients are updated at the end of each assimilation and are used as inputs in the subsequent analysis cycle.

Second, a scan-dependent bias correction is applied and updated in-line with the GSI using an offline program. This determines a bias estimate as a function of the scan position for each satellite instrument, channel, and platform. These corrections are updated using the analysis departures (observation minus the predicted observation in the final analysis) of the observations that passed

quality control after the completion of each analysis and are also used as inputs for the subsequent analysis cycle.

Radiances from the GOES sounders and two SEVIRI water vapor channels are also assimilated. These are considered to have large observation errors, however, and have limited impact on the analysis.

The nominal channel selections for each instrument type are shown in Table 3. For the microwave temperature sounders, only channels that peak above the surface are considered. For microwave humidity sounders, window channels are actively assimilated along with the sounding channels. For ATMS, which has both temperature and moisture sounding channels, channel 16 (88.2 GHz) is excluded, which is consistent with the treatment of surface-sensitive channels on other temperature sounding instruments. The highest peaking channels for AMSU-A (channel 14) and ATMS (channel 15) are assimilated without bias correction. These channels are sensitive to upper-stratosphere and lower-mesosphere temperature. Bias correction is not applied for two reasons. First, the channel acts as an anchor for all observations within a given footprint, as there are no independent observations at these heights (> ~50 km) to prevent the bias correction from drifting in an unconstrained manner. Second, the background state at these levels has large biases, as physical processes in the mesosphere are not properly accounted for in the model. The bias correction terms, which correct the brightness temperature background departure (observed minus forecasted) and not the observation itself, might again drift significantly (Dee and Uppala 2008).

Similarly, channel 3 on SSU, which peaks at approximately 1 hPa, is also assimilated without bias correction. SSU Channel 3 and AMSU-A Channel 14 are fundamentally different in that the SSU measured in the infrared via a pressure modulation cell approach, whereas AMSU-A measures passively in the microwave. The differences result in AMSU-A channel 14 being comparatively less sensitive to the lower mesosphere temperature biases present in the background – a result of having a narrower weighting function. Due to these differences, there is no overlap in these observations as SSU Channel 3 is disabled with the introduction of NOAA-15 AMSU-A on 1 Nov 1998.

For infrared sounders, temperature observations from the 15 μm CO_2 absorption continuum, surface channels from the 11 μm atmospheric window, and the 6 μm water vapor absorption region are assimilated. Radiances from IASI are used differently from those of AIRS and CrIS in that only CO_2 and surface channels are assimilated. For all infrared instruments, observations sensitive to ozone (9.6 μm) are excluded. Observations sensitive to the 4 μm spectral region are excluded in MERRA-2, with the exception of AIRS, for which 14 channels from 4.4 to 4.6 μm are assimilated.

2.3.2 GPS Radio Occultation

GPS radio occultation (GPSRO) observations of bending angle (Cucurull et al. 2013) are assimilated up to 30 km in MERRA-2. Assimilation of these data begins with the introduction of the Challenging Minisat Payload (CHAMP) platform on 15 July 2004[2] and continues into near-

[2] CHAMP data was inadvertently excluded between 19 May 2001 and 14 Jul 2004

Satellite Radiance Usage (Nominal)	
Instrument	Channels Assimilated
Microwave Sounding Unit	2 - 4
Advanced Microwave Sounding Unit-A	4 - 13, 14
Advanced Technology Microwave Sounder	5 - 14, 15, 17 - 22
Advanced Microwave Sounding Unit-B	1 - 5
Microwave Humidity Sounder	1 - 5
Special Sensor Microwave Imager	1 - 7
Stratospheric Sounding Unit	1, 2, 3
High-resolution Infrared Radiation Sounder	2 - 8, 10 - 12
Atmospheric Infrared Sounder	See Appendix A
Infrared Atmospheric Sounding Interferometer	See Appendix A
Cross-Track Infrared Sounder	See Appendix A
Geostationary Operational Environmental Satellite Sounder	1 - 8, 10 - 12
Spinning Enhanced Visible and InfraRed Imager	2, 3

Table 3 - The nominal channel selections by instrument for the satellite radiances assimilated in MERRA-2. Channels in red denote those that are assimilated without any bias correction.

real time (Figure 1). These observations provide primarily temperature information and play an important role in constraining the variational bias correction procedure applied to satellite radiances (Healy 2008). The number and coverage of GPSRO observations increased significantly with the introduction of the joint Taiwan - U.S. Constellation Observing System for Meteorology, Ionosphere, and Climate (COSMIC) on 13 July 2006, with subsequent increases provided by GPSRO payloads on Metop-A and -B, Gravity Recovery and Climate Experiment (GRACE), Satélite de Aplicaciones Científicas-C/Scientific Application Satellite-C (SAC-C), and TerraSAR-X.

2.3.3 Satellite Retrievals of Temperature

Retrieved temperature profiles from the Microwave Limb Sounder (MLS) on the NASA Earth Observing System (EOS) Aura satellite (Schwartz et al. 2008) are assimilated as point temperature observations in MERRA-2 beginning on 13 August 2004 and continuing into near-real time. Version 3.3 retrievals (Livesey et al. 2013b) are assimilated before 1 June 2015, and version 4.2 (Livesey et al. 2015) are assimilated thereafter. Only observations at and above 5 hPa (~40 km) are assimilated, since lower altitudes are well observed by other satellite and conventional data. The counts for these observations are shown in Figure 2.

2.3.4 Satellite Retrievals of Rain Rate

Rain rate retrievals from SSM/I (Goddard Profiling Algorithm, or GPROF, Kummerow et al. 2001) and the Tropical Rainfall Measuring Mission (TRMM) Microwave Imager (TMI) are assimilated in MERRA-2 using the methods presented in Treadon et al. (2002). Assimilation of the SSM/I data begins 9 July 1988 and continues through 16 Sept 2009. Retrievals from the DMSP F8, F10, F11, F13, and F14 satellites were used. Rain rate retrievals from the TMI retrieval algorithm Version 6 (collection 2A12, Olson et al. 2006, Yang et al. 2006) were assimilated beginning 1 Jan 1998. On 1 July 2011, the TMI retrieval assimilation switched to Version 7 processing, and the retrievals were assimilated to the end of the TRMM mission on 8 April 2015. These observations are generally few in number (Figure 1) and have been shown to provide minimal impact on the analysis.

2.3.5 Ozone Retrievals

Prior to 1 October 2004, ozone observations assimilated into MERRA-2 are from the Solar Backscatter Ultra Violet Radiometers (SBUV and SBUV/2 – collectively referred to as SBUV hereafter) flown on NASA Nimbus-7 and several NOAA POES satellites. MERRA-2 uses version 8.6 retrievals of partial column ozone on 21 layers (Frith et al., 2014, McPeters et al., 2013), each approximately 3 km deep. Also assimilated is the total ozone column obtained by summing all the layers at a given observation location. The assumed total ozone observation error is set to a constant value of 6 Dobson Units (~2 % of the average global total ozone). The observation errors for SBUV partial columns are specified to be ~1.5 Dobson Units per layer up to 3 hPa, and 1 Dobson Unit above this level.

The combined SBUV observations provide a nearly continuous record of global ozone from the beginning of the era of satellite measurements to the present. The only significant gap occurs in

March 1991 when no SBUV observations were available for the entire month. The timelines of the NOAA and Aura platforms are shown in Figure 6.

Beginning 1 October 2004 the SBUV data were replaced in MERRA-2 by stratospheric profiles from the Microwave Limb Sounder (MLS, Waters et al. 2006) instrument and total ozone column observations from the Ozone Monitoring Instrument (OMI), both on NASA's Earth Observing System Aura (EOS Aura) satellite. The physical principles of measurement, retrieval algorithms, and resulting data characteristics (coverage, resolution and patterns of sensitivity in the vertical) are fundamentally different between SBUV and MLS. The decision to switch from SBUV to EOS Aura observations once the latter became available was based on the desire to use the most advanced data available.

The system configuration for the EOS Aura data is similar to that described and extensively validated by Wargan et al. (2015), with the main differences being the inclusion of a simple parameterization of tropospheric ozone chemistry in MERRA-2 and the use of different versions of MLS retrievals. In MERRA-2, MLS ozone profiles are assimilated from version 2.2 retrievals (Livesey et al. 2013a) starting in 2004 and from version 4.2 (Livesey et al. 2016) beginning 1 June 2015. Following Wargan et al. (2015) a mid-level averaging algorithm is applied prior to assimilation of the version 2.2 data, but no averaging is performed after the switch to version 4.2. OMI collection 3, version 8.5 total column ozone data retrievals (Levelt et al. 2006) are also assimilated. As for SBUV, a constant OMI total ozone observation error of 6 Dobson Units is assumed.

3. Selected Observation Assessment

3.1 Radiosonde Temperature and Wind

The monthly mean and root mean squared (RMS) background departures for radiosonde temperature are shown in Figure 7 at 200, 500, and 850 hPa. At 200 hPa, there is a marked increase in negative bias beginning in 1998. For this discussion, annual means are used to help quantify the interannual shifts. The annual mean departure at this level increases from -0.08 K in 1998 to a peak value of -0.50 K in 2003. It decreases in magnitude beginning in 2008 and stabilizes to around -0.3 K by 2010. The increased bias at this level correlates with the increase in the number of satellite radiances and aircraft observations during the late 1990's (Figure 2). It is noted that these observations are bias corrected as discussed in sections 2.3.1 and 3.2 for the radiances and aircraft, respectively. This, combined with a warm upper tropospheric model bias (Molod 2016, personal communication), contributes, in part, to this negative bias. Further assessment of this is available in Gelaro et al. (2016).

There is also a negative bias at 500 hPa, although its increase in magnitude is more gradual and begins prior to the increase in the number of aircraft observations. Specifically, the annual mean background departure at this level increases from -0.09 K in 1991 to its largest magnitude of -0.31 K in 2003. The mean departure is reduced from 2006 onward, corresponding to the increase in GPS radio occultation observations. The mean background departure at this level stabilizes to between -0.11 and -0.13 K after 2010. At 850 hPa, the annual mean background departure is more consistent from 1980 to 2005, ranging from 0.0 K in 2002 to 0.1K in 1991. An

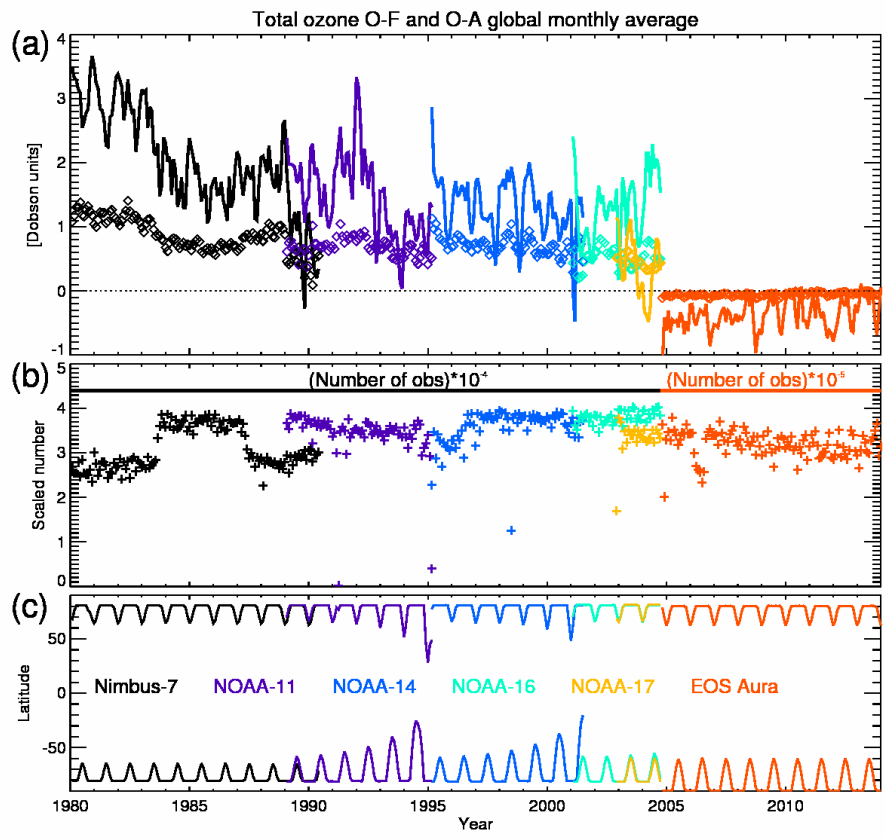

Figure 6 - Time series of various quantities relevant to the total ozone column observations in MERRA-2. (a) The global mean monthly background (solid) and analysis (diamonds) departures. March 2001 was excluded because SBUV observations were not available then except for 0000 UTC on 1 March 2001. (b) Monthly data counts; note that the counts for OMI (annotated by orange line) are scaled down by a factor of 10 relative to SBUV (annotated by black line). (c) The monthly extent of total ozone observations (the highest observed latitudes).

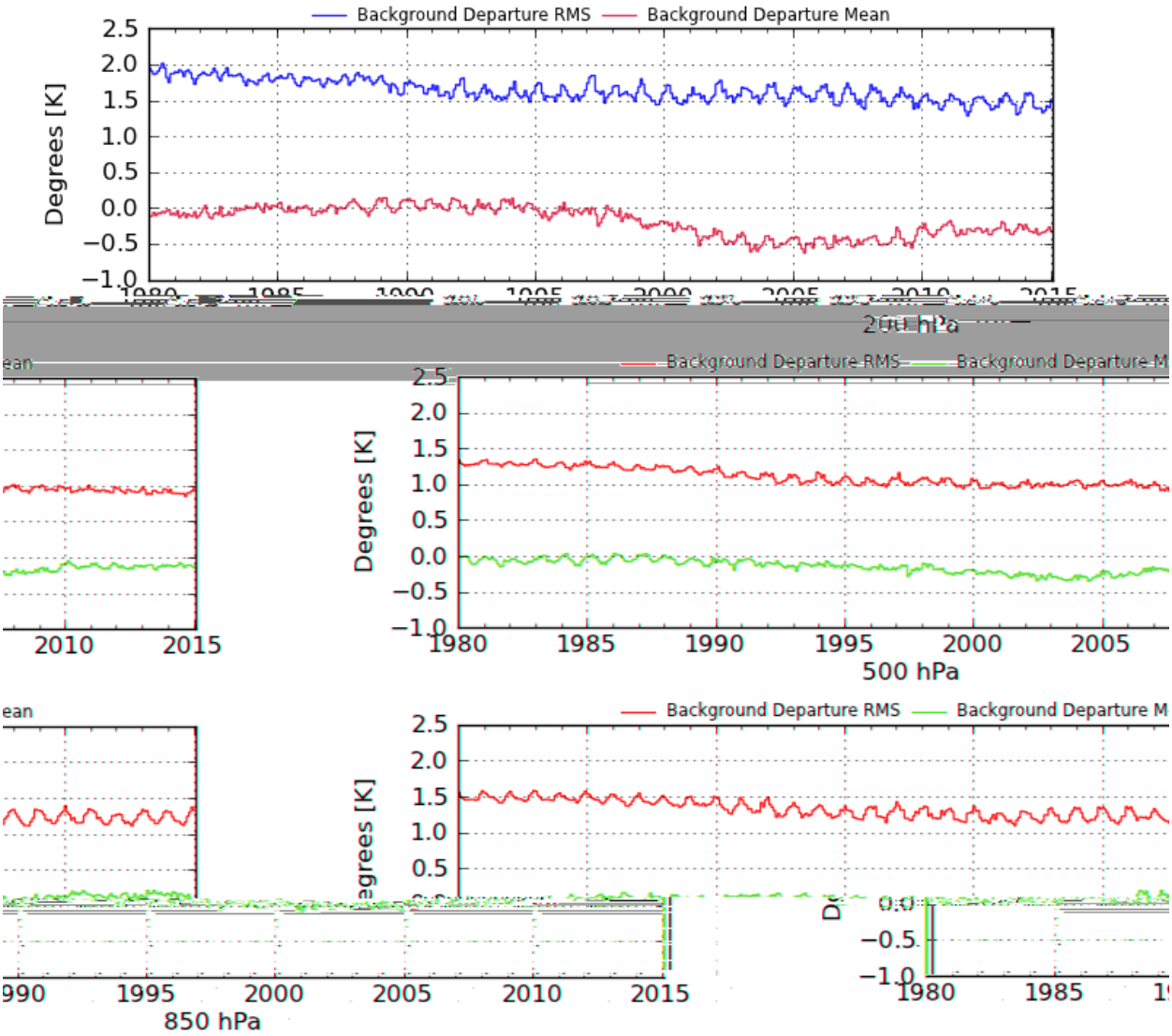

Figure 7 - The monthly mean (red) and root mean squared difference (blue) of the radiosonde temperature background departures at 200 (top), 500 (middle), and 850 (bottom) hPa.

increased bias is seen beginning in 2006, as the annual mean background departure ranges from 0.08 K in 2008 to 0.16 K in 2010 and 2013. The RMS for the three levels (Fig. 7, blue) is largest in the earliest periods and decreases through the 1980s before becoming more stable in the early 1990s. Relative to 1980, the annual mean RMS is decreased by 16%, 21%, and 15% at 200 hPa, 500 hPa, and 850 hPa, respectively, by 1996. These metrics are further reduced to 23%, 30%, and 17%, again relative to 1980, by 2014.

The monthly-averaged background departure mean and RMS for radiosonde winds are shown in Figure 8. The mean background departures are generally stable over the MERRA-2 period. At 200 hPa, the annual mean wind departure varies from -0.18 to 0.11 ms^{-1} in 1996 and 1986, respectively. At 500 hPa, the annual mean departure varies from -0.01 to 0.10 ms^{-1} in 2013 and 2003, respectively. At 850 hPa, the annual mean departure varies from 0.02 to 0.12 ms-1 in 1989 and 2001, respectively. The annual mean RMS for radiosondes is 3.93, 3.20, and 2.61 ms-1 in 1980 at 200, 500, and 850 hPa, respectively. At all levels, the RMS decreases monotonically until 1993, when the RMS at the three levels has decreased respectively by 9.0%, 4.5%, and 4.6% of the 1980 values. The RMS at all three levels decreases from 1993 onward, although by this time the rate of decrease is comparatively slower at 850 hPa. By 2014, the RMS values are reduced by 14.6%, 14.2%, and 7.1% of the 1980 values at 200, 500, and 850 hPa.

3.2 Aircraft Temperature and Bias Correction

The MERRA-2 aircraft temperature bias correction uses the mean temperature background departures to estimate the bias for temperature reports from individual aircraft, as identified by the tail numbers that are reported as the observation station identifier. The bias correction is only calculated for AMDAR and ACARS reports; other aircraft did not report unique tail numbers/station identifiers and could not be tracked. Temperature reports below 600hPa, as well as reports where the aircraft appear to be rapidly ascending or descending, are excluded. During periods when a tail number is not reporting, the background error for the bias coefficient is inflated; the correction for the tail number is eventually dropped after an extended period without observations.

Figure 9 shows an example of the bias estimate for temperature measurements from one aircraft over three of the MERRA-2 streams. The bias exhibits gradual variations punctuated by sudden shifts, to which the scheme adjusts fairly quickly. Figure 10 shows the bias estimate for this tail number during the overlap period of the second and third MERRA-2 streams, which begin in 1991 and 2000, respectively. At the beginning of the third stream (after the initial spinup) the bias estimate is slightly more positive than at the end of the second stream. This illustrates the influence of the background temperature difference between the two streams on the bias estimate. The estimates for other aircraft generally show similar behavior during overlap periods.

Overall, the aircraft bias correction procedure reduces the bias between the corrected aircraft observations and the forecast background. It also reduces the variance of temperature background departure by filtering the measurement ‘noise’ associated with individual aircraft temperature sensors. This is illustrated in Figure 11, which shows the distribution of background departures for ACARS and AMDAR reports before and after bias correction.

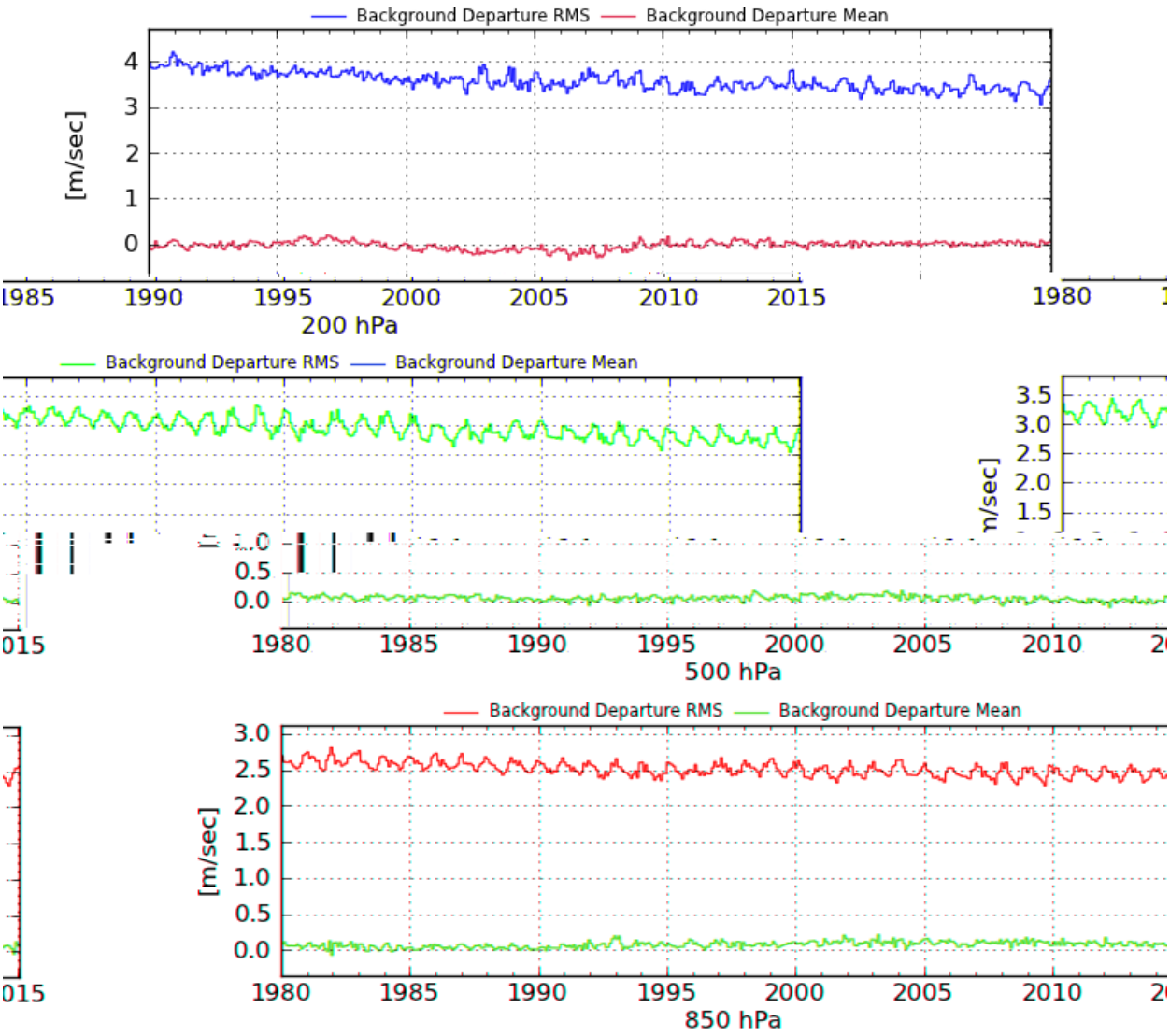

Figure 8 - Same as Fig. 7, except for radiosonde wind.

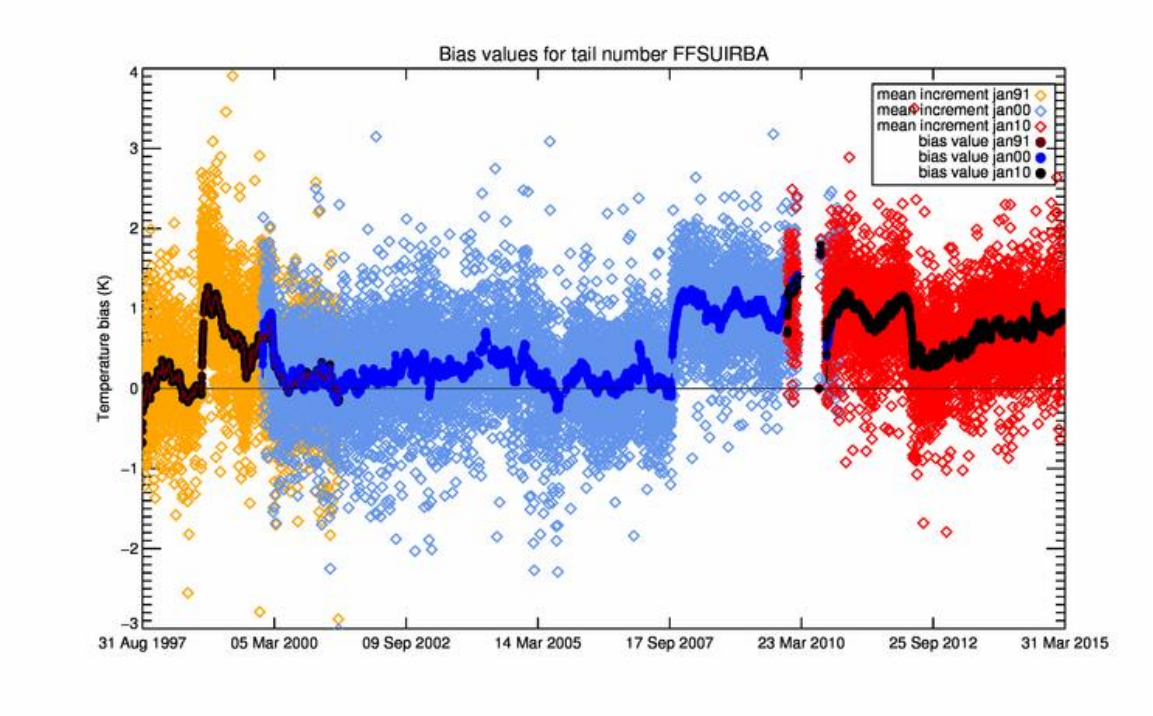

Figure 9 - Aircraft bias correction for ACARS tail number FFSUIRBA. Open diamonds – mean (O-F) temperature above 600hPa at each synoptic time. Filled circles: updated bias estimate. Orange diamonds/dark brown circles – 1991 stream. Light blue diamonds/blue circles – 2000 stream. Red diamonds/black circles – 2010 stream.

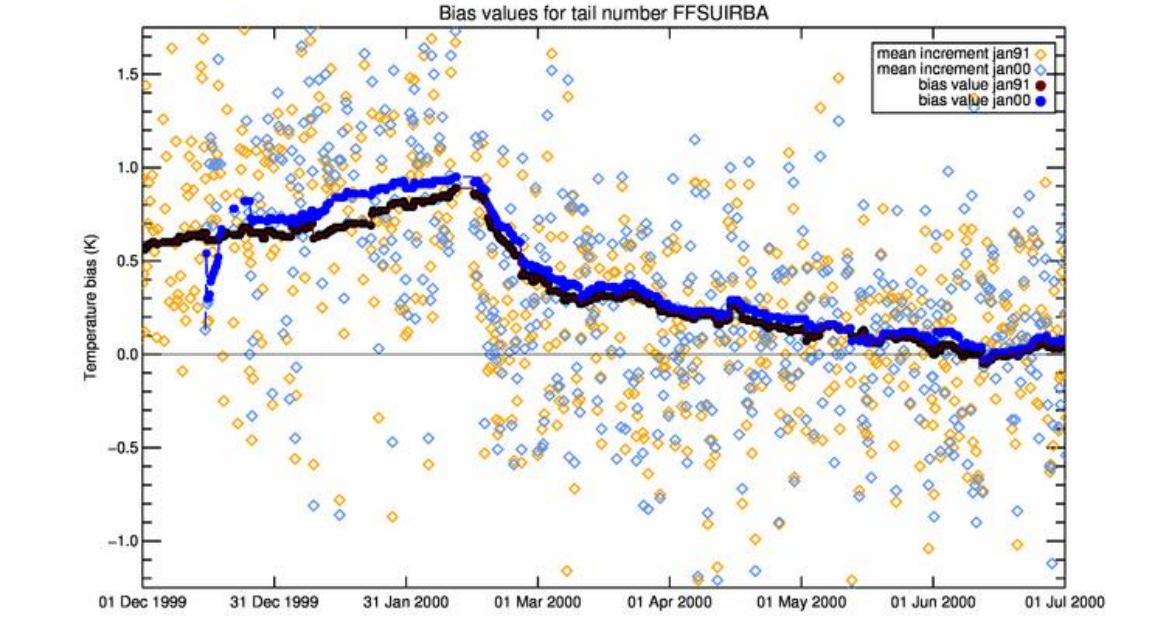

Figure 10 - Aircraft bias correction as in Figure 9, for the overlap between the second (1991) stream and third (2000) stream.

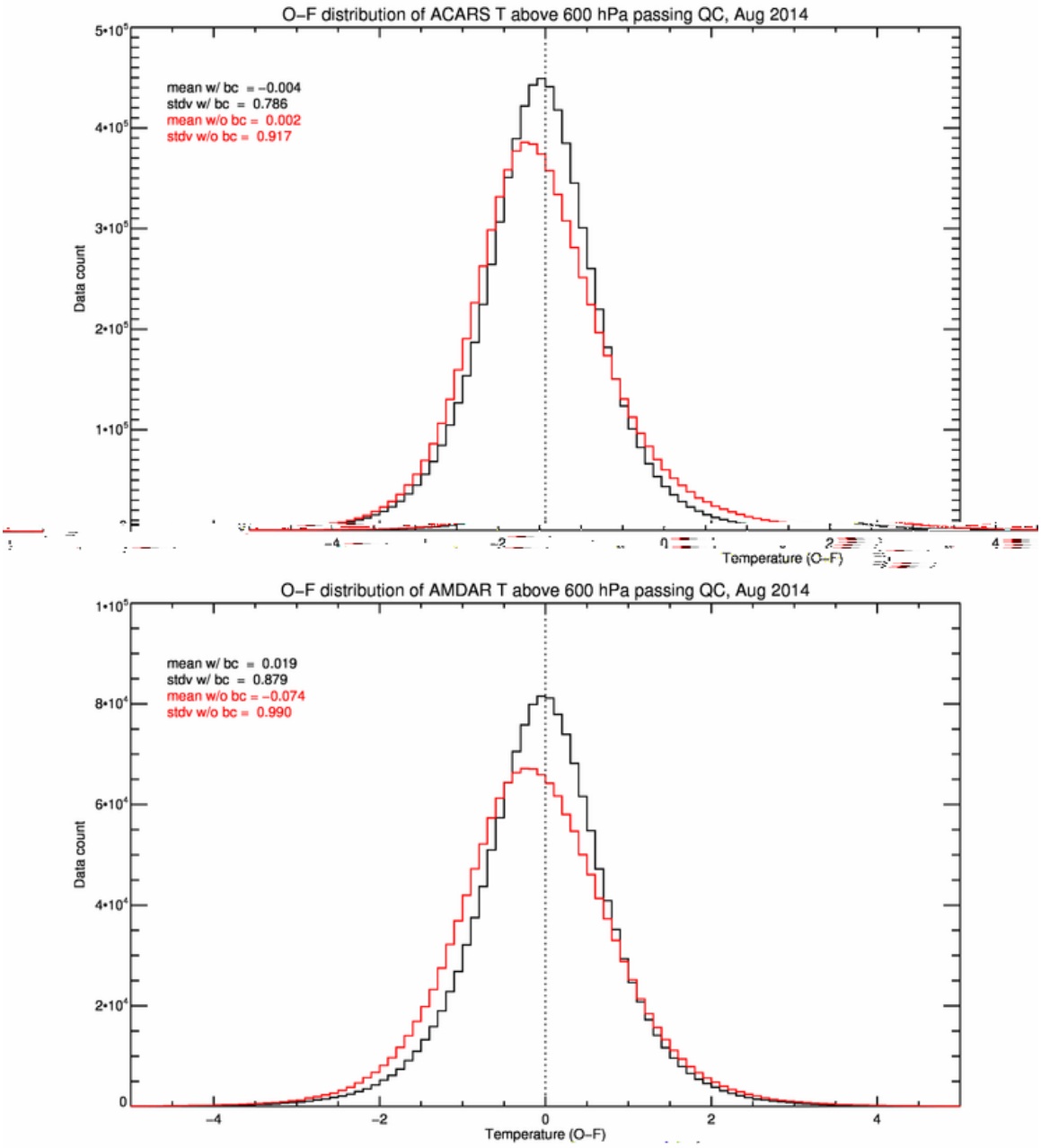

Figure 11 - Histogram of ACARS (top) and AMDAR (bottom) aircraft temperature background departures with (black) and without (red) bias correction.

3.3 Satellite Winds - Atmospheric Motion Vectors

The atmospheric motion vectors described in Section 2.2 are derived from both geostationary (Fig. 3: NOAA, JMA, and EUMETSAT) and polar orbiting (Fig. 3: NOAA/EUMETSAT AVHRR and NASA MODIS) satellites. The latter are often referred to as "polar winds" because they provide coverage at latitudes generally poleward of 60 degrees.

The background departure monthly mean and RMS for the geostationary AMVs at selected levels is shown in Figure 12. Prior to 1982 the AMVs exhibit notable biases and RMS at 500 and 700 hPa. These correspond to very low observation counts (Fig. 3). At 500 hPa, the magnitudes of the departure mean and RMS decrease from -0.30 and 3.71 ms^{-1}, respectively, between 1980 and 1981 to 0.06 and 2.69 ms^{-1}, respectively, in 1983. In 1987, there is increased interannual variability of the mean, while the RMS increases to 3.61 ms^{-1}. At 700 hPa, the mean and RMS decrease from -0.93 and 3.58 ms^{-1}, respectively, between 1980 and 1981 to -0.12 and 2.53 ms^{-1}, respectively, in 1983. At 300 hPa, the RMS values exhibit significant interannual variability prior to 1998.

The departure values at all three levels exhibit a noticeable change in character after high resolution GOES AMVs enter the system on 11 Mar 1998 (Figure 3). After this time, the mean and RMS values at all levels exhibit less month-to-month variability. In addition to being of higher quality, the GOES AMVs dominate the statistics in terms of count. The March 1998 transition also marks the first assimilation of water vapor AMVs in MERRA-2. Prior to this, only cloud-tracked AMVs in the infrared window (~11 μm) bands were assimilated.

The monthly mean and RMS for polar AMV background departures at 500 hPa is shown in Figure 13. In Oct 2009, there was an update to the AVHRR AMV processing. Prior to the switch, AVHRR AMVs, which are only derived from cloud tracks in the infrared window, showed a consistently positive bias and larger RMS. The annual mean departure decreases from 0.26 to 0.03 ms^{-1} from 2008 to 2010. The annual RMS for these observations decreases from 3.42 to 2.88 ms^{-1} over the same period. Prior to 1 Oct 2004, an older version of MODIS AMVs was used, and the statistics are degraded compared to those obtained with newer versions. The mean departure for the MODIS cloud-track and water vapor AMVs between 2005 and 2008 is -0.02 and -0.01 ms^{-1}, respectively. The RMS for the MODIS cloud-track and water vapor AMVs is 2.67 and 2.63 ms^{-1}, respectively, over this period. Both statistics react to the introduction of the improved AVHRR observations. The bias increases slightly in magnitude to -0.05 ms^{-1} over the period of 2010-2014 for both the water vapor and infrared AMVs, and the RMS decreases to 2.54 and 2.58 ms^{-1}, respectively.

3.4 Satellite Winds – Surface Winds

The background departure monthly mean and RMS for the satellite-derived surface wind observations described in Section 2.2 are shown in Figure 14. The mean departures show that the surface wind vector observations from WindSat and the scatterometers exhibit very small biases over time, generally ranging between 0.0 and -0.1 ms^{-1}. A notable exception to this is ERS2 data after 2003. This is an artifact of poor spatial sampling, as only observations measured when the satellite was in line-of-sight to a ground station were obtainable due to a failure of the satellite's

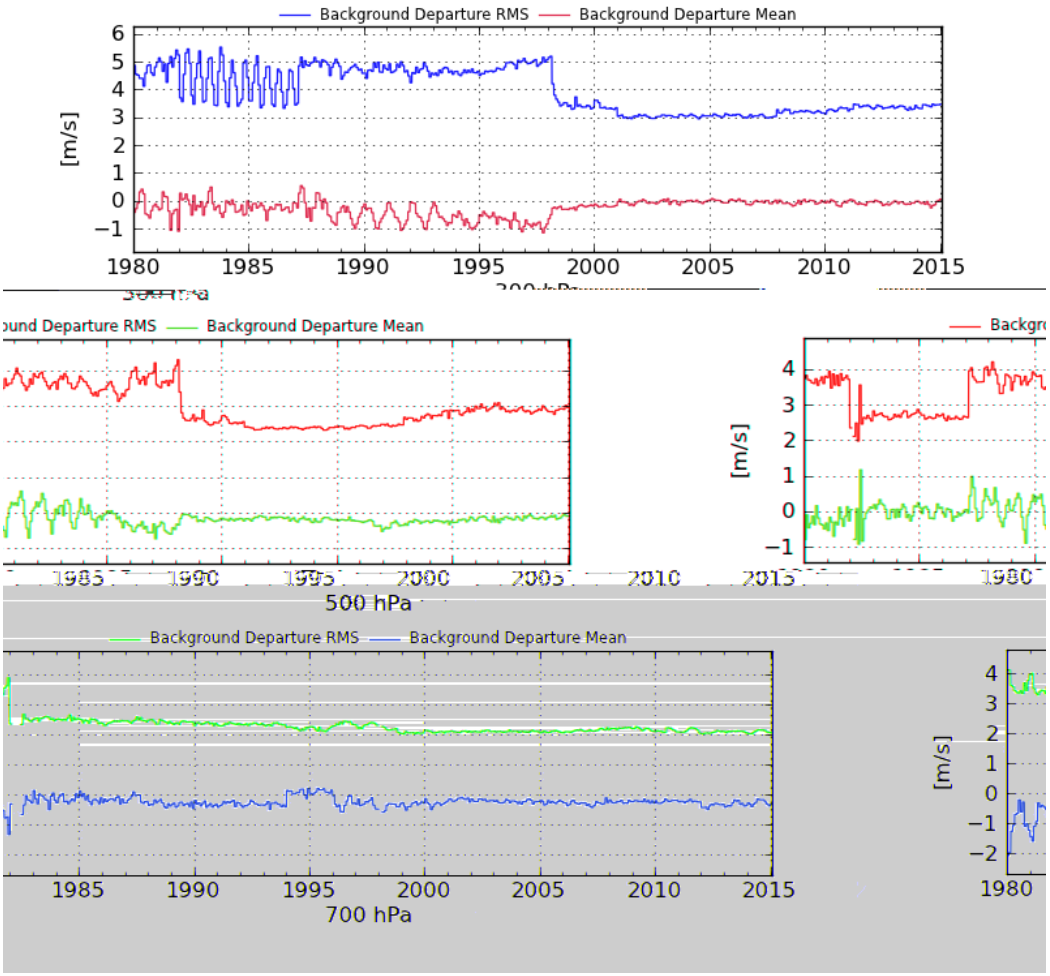

Figure 12 - The monthly mean (red) and root mean squared difference (blue) of the background departure for all geostationary wind types at 300 hPa (top), 500 hPa (middle), and 700 hPa (bottom).

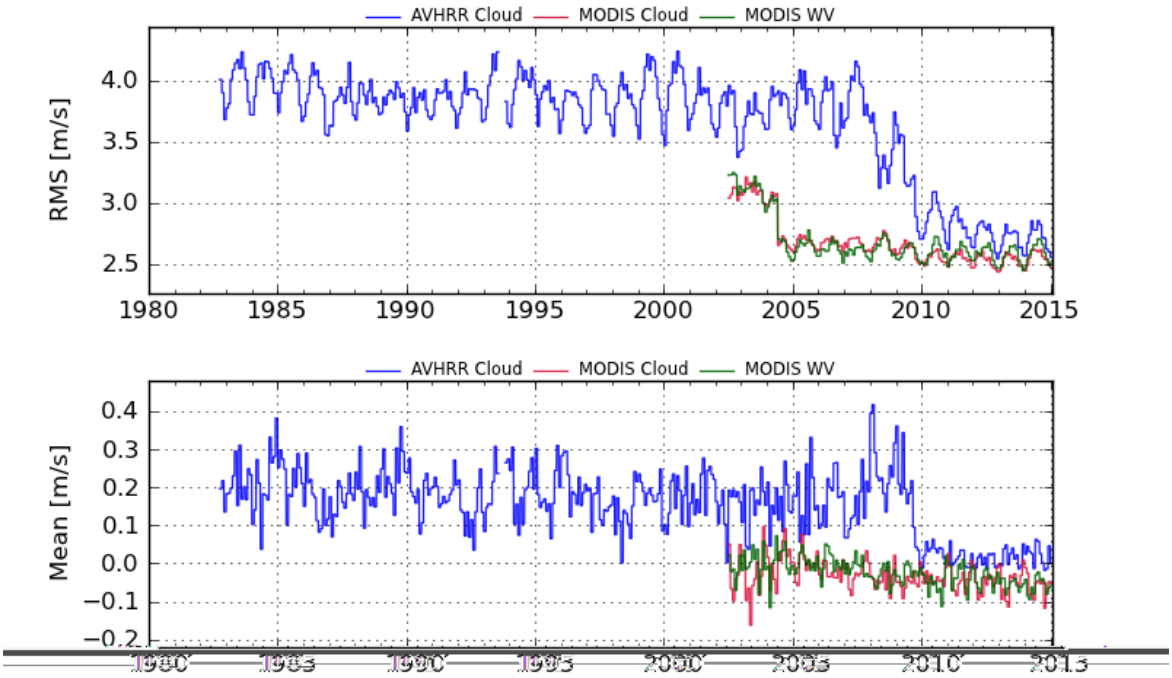

Figure 13 - The background departure monthly RMS (top) and mean (bottom) for AVHRR cloud-track (blue), MODIS cloud-track (red), and MODIS water vapor (green) polar AMVs.

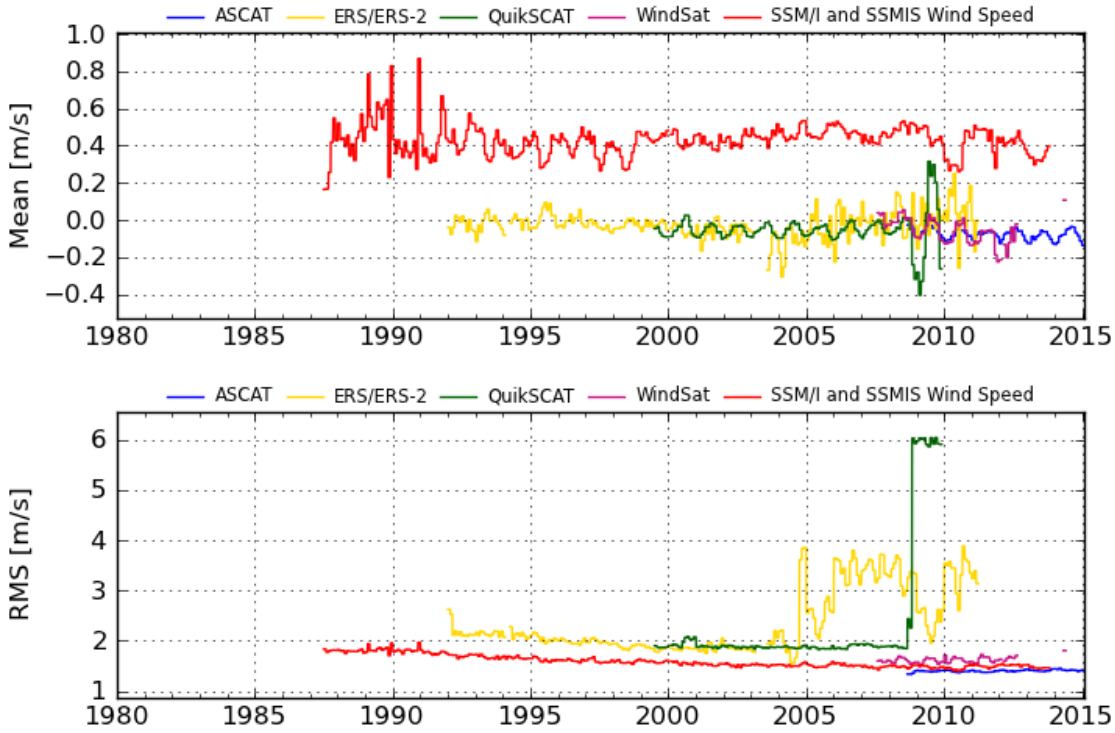

Figure 14 - The background departure monthly RMS (top) and mean (bottom) for satellite-retrieved surface vector winds from ASCAT (blue), ERS & ERS-2 (yellow), QuikSCAT (green), and WindSat (purple), as well as for SSM/I & SSMIS retrieved wind speed.

onboard storage. Another notable change in character occurs at the end of the QuikSCAT record in November 2008, as the data became more variant and biased. While there is no apparent reaction in the WindSat or ASCAT background departure mean or RMS, this change in character will likely prompt the exclusion of these QuikSCAT observations from future reanalyses.

For SSM/I and SSMIS retrieved wind speed observations, the month-to-month variability of both the background departure mean and RMS becomes more stable with the introduction of DMSP F10 on 12 Feb 1991. Both 85.5 GHz bands on DMSP F08, which are important for quality control of the retrieval, failed shortly after launch. This likely explains the fact that SSM/I and SSMIS wind speeds exhibit a positive bias relative to both the model and scatterometer observations, which are unbiased relative to each other. The bias over the entire SSM/I and SSMIS wind speed record is 0.43 ms^{-1}. The RMS of these observations decreases over time from 1.82 ms^{-1} between 1988 and 1990 to 1.50 ms^{-1} between 2006 and 2008.

3.5 Microwave Sounding Unit Radiances

The Microwave Sounding Unit (MSU) provides the bulk of global tropospheric observations prior to 1998. Beginning on 1 Nov 1986, recalibrated radiances (Zou et al. 2006) were used; uncorrected measurements were used prior to this. The consistency of these observations has been assessed in various studies (e.g. Zou and Wang 2010) as they are central to climate research.

Time series of the mean observed brightness temperature of MSU channel 3 assimilated observations (Fig. 15, upper-right, top) show clear differences among overlapping platforms, most notably prior to the use of the recalibrated observations. The differences are less apparent for channels 2 and 4 (Fig. 15, upper-left and lower-left, respectively), although for channel 4, NOAA-9 spikes towards the end of its life. For channel 3, the mean background departures, in contrast, show more stability and better inter-platform agreement (Fig. 15, upper-right, middle) because the bias correction (Fig 15, upper-right, bottom) accounts for most of the calibration differences between satellites.

3.6 Stratospheric Sounding Unit Radiances

The Stratospheric Sounding Unit (SSU) provides a significant amount of temperature information in the stratosphere prior to the ATOVS period. These data are especially important in the middle and upper stratosphere, with channels 1, 2, and 3 having peak sensitivities at approximately 13, 4, and 1 hPa, respectively. For comparison, the sensitivity of MSU channel 4 peaks at 80 hPa and HIRS/2 channel 2 peaks at 58 hPa. SSU channel 3 is not bias corrected in MERRA-2 for two reasons. First, because of the formulation of the variational bias correction scheme, large model biases present in the lower mesosphere would induce an erroneous correction of the observations at these levels. Second, channel 3 acts as an anchor for other observations as it prevents the bias correction for all channels to drift over long time periods (Dee and Uppala 2008). Unfortunately, for certain periods during MERRA-2, channel 3 was erroneously bias corrected due to misconfiguration of the system. Specifically, bias correction was applied to SSU channel 3 for:

- NOAA-6 between 2-4 Mar 1980,
- NOAA-6 between 4-5 Nov 1980,
- NOAA-7 on 2 March 1984,

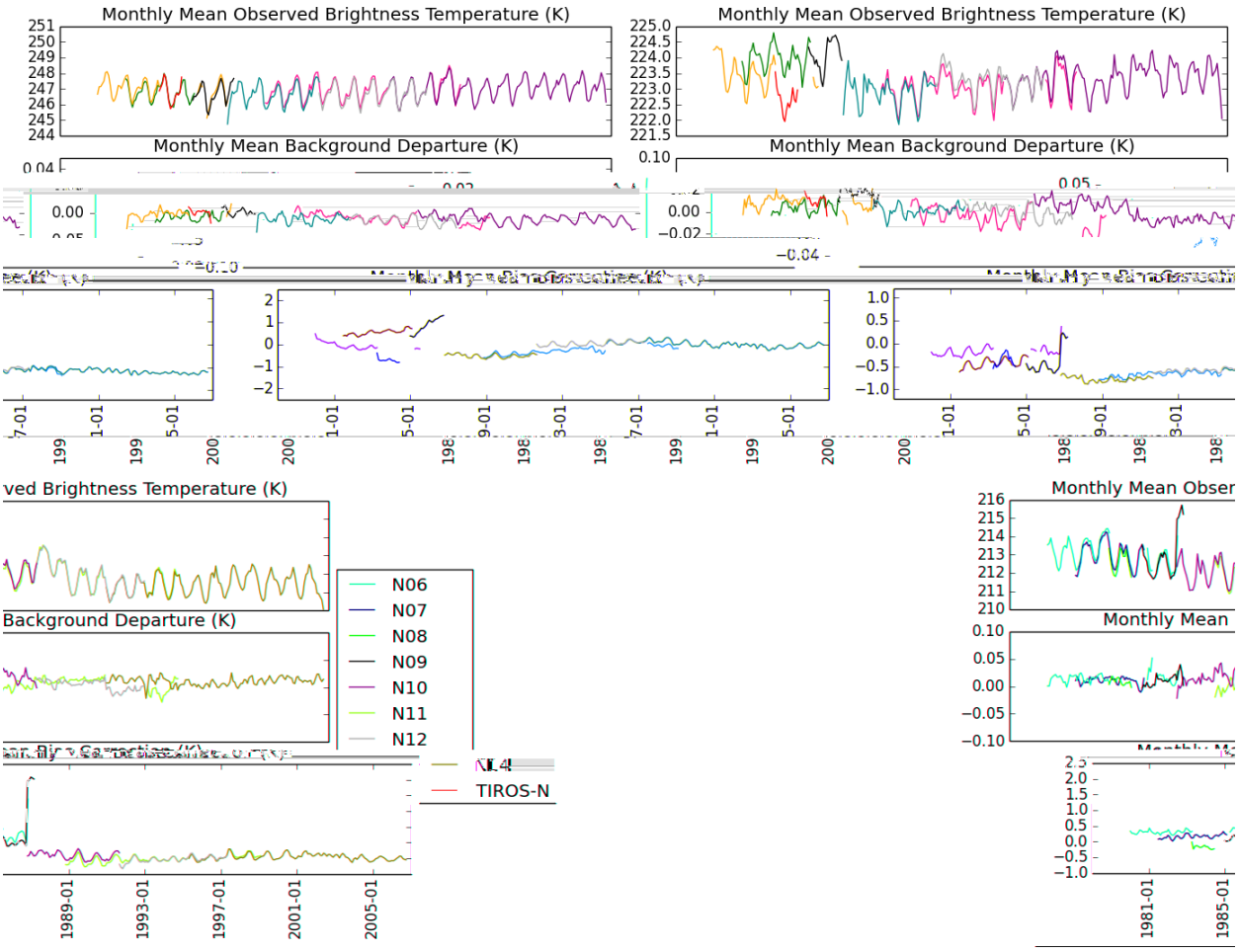

Figure 15 - Microwave Sounding Unit Channel 2 (upper-left), Channel 3 (upper-right), and Channel 4 (lower-left) monthly mean observed brightness temperatures (top), bias corrected background departure (middle), and bias correction (bottom).

- NOAA-6 between 1 Nov 1985 – 2 Jan 1986,
- NOAA-9 between 1 - 2 Jan 1986,
- NOAA-9 between 1 - 2 Jan 1987,
- NOAA-9 between 2 – 7 Nov 1988,
- NOAA-11 between 28 Sept - 2 Nov 1988, and
- NOAA-14 on 30 April 1996.

The performance of channel 1 is mostly consistent across platforms in terms of both the observed brightness temperatures (Fig 16, upper-left, top) and background departures (Fig. 16, upper-left, middle). One exception is the inconsistency between the background departures for TIROS-N and NOAA-6, which differ by approximately 0.05 K over the short life of the TIROS-N instrument. A second is the inconsistency between the departures for NOAA-11 and NOAA-14. Upon the switch from NOAA-11 to NOAA-14 in Jan 1995, the departures for channel 1 change sign from slightly negative (~0.02 K for NOAA-11) to slightly positive (~ 0.03 K for NOAA-14). When NOAA-11 re-enters operations in July 1997, its negative bias increases to approximately 0.06 K. Disregarding seasonal variability, the bias corrections for channel 1 are generally negative (with the exception of TIROS-N) and range from -0.3 K to -1.0 K (Fig. 16, upper-left, bottom).

For Channel 2, there is a gap in the data record from 20 Jun 1984 to 1 Jan 1985. This channel exhibits inconsistencies between platforms early in the period including, for example, the visible trend in mean brightness temperature for NOAA-7 (Fig. 16, upper-right, top). The SSU is known to have had a leak in its CO_2 cell pressure that resulted in an unstable calibration and downward progression over time of the weighting function for channel 2. As mentioned in section 2.3.1, the CRTM attempts to account for this effect (Chen et al. 2011), but there is still a trend visible in the bias correction for NOAA-7 (Fig. 16, upper-right, bottom) that appears correlated to this known issue. As in the case of channel 1, the background departures for NOAA-11 and NOAA-14 differ noticeably both at the transition between satellites in January 1995 and after the reintroduction of NOAA-11 in July 1997 (Fig. 16, upper-right, middle).

For channel 3, there are notable inconsistencies between platforms, as no bias correction is routinely performed (see above) to adjust these observations. Figure 16 (lower-left, top) shows a clear difference in the mean observed brightness temperatures between the early observations (TIROS-N, NOAA-6, and NOAA-7) and the later observations (NOAA-9 onward). Background departures are sensitive to the introduction and removal of other platforms due to the lack of bias correction. This is most apparent for NOAA-6, as the mean of the background departures (Fig. 16, lower-left, middle) shift by 0.4 K with the introduction of NOAA-7 observations in July 1981. As mentioned above, there were some periods when bias correction was performed on these observations, and these periods are apparent in Figure 16 (lower-left, bottom).

3.7 Advanced Microwave Sounding Unit-A Radiances

The Advanced Microwave Sounding Unit-A (AMSU-A) microwave radiometer was introduced in November 1998 and remains a core component of the modern observing system. Six AMSU-A instruments are still functionally assimilated in MERRA-2 as it progresses in near-real time. Beginning with NOAA-15, this instrument provides advancements beyond the MSU/SSU suite, shifting stratospheric observations to the microwave and increasing the number of available

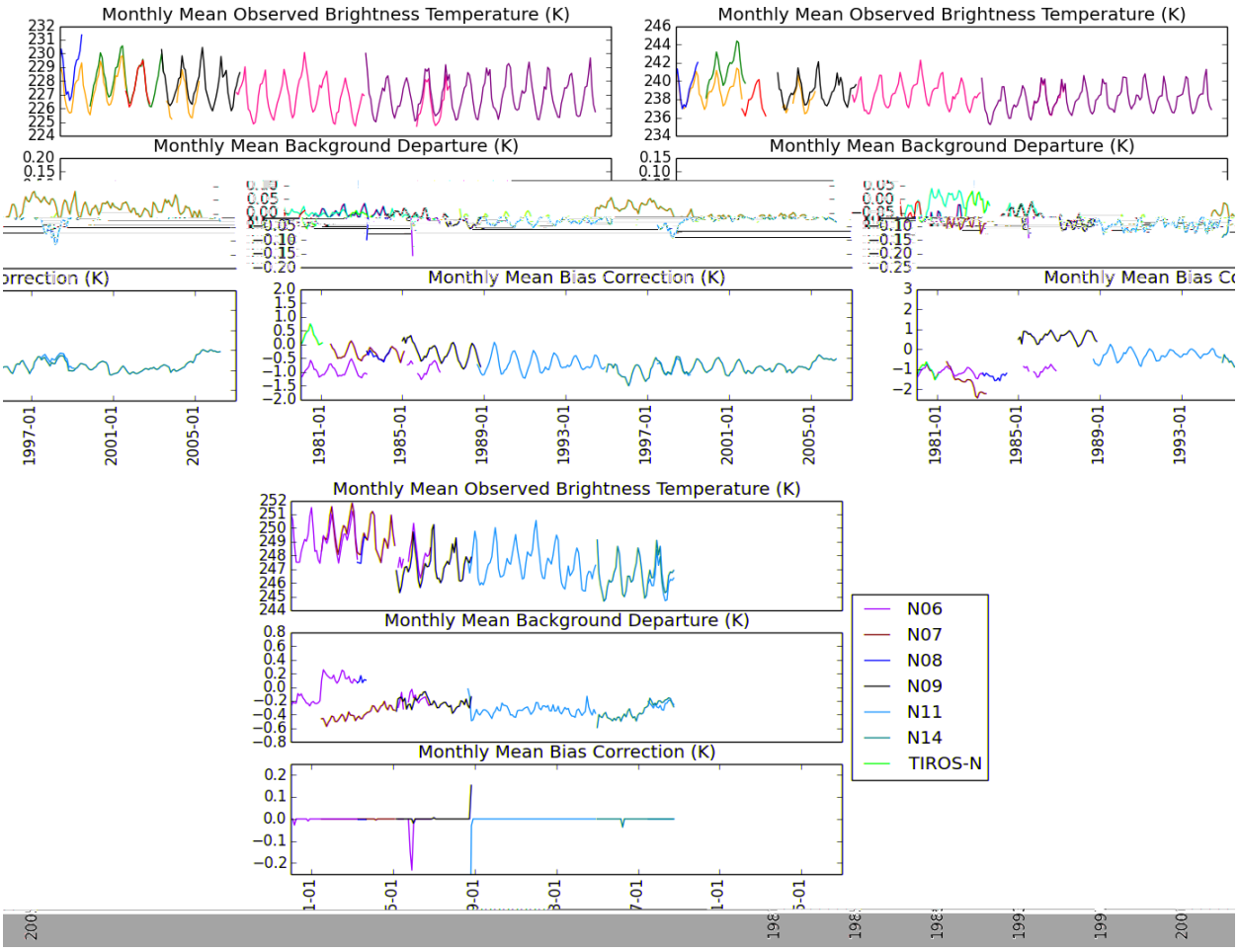

Figure 16 - Same as Figure 15, but for Stratospheric Sounding Unit Channel 1 (upper-left), Channel 2 (upper-right), and Channel 3 (lower-left).

channels from 7 (on MSU and SSU combined) to 15. The full timeline of AMSU-A instruments is shown in Figure 5, although it is noted that some channels have failed over the course of data record.

Time series of monthly-mean brightness temperatures, background departures, and bias corrections are shown for channels 5, 7, and 9 in Figure 17. These channels were selected because they are analogous to MSU channels 2-4 in that the weighting functions for AMSU-A (MSU) channels 5 (2), 7 (3), and 9 (4) peak at approximately 650 (585) hPa, 241 (229) hPa, and 92 (80) hPa, respectively. Accordingly, the results in Figure 17 are qualitatively comparable to those in Figure 15.

For all channels, NOAA-15 and NOAA-16 show a larger disagreement in mean brightness temperature (Fig. 17) compared with other AMSU-A instruments. Compared to the mean observed brightness temperature for AMSU-A channel 5 on NOAA-17-onward (Fig. 17, upper-left, top), NOAA-15 and NOAA-16 are warmer by 1.5 K and 0.6 K, respectively, over their entire record. A similar feature is seen in channels 7 and 9 (Fig. 17, upper-right, top and lower-left, top, respectively). However, these differences are mostly accounted for by the variational bias correction procedure such that the resulting background departures for all platforms and channels are on the order of hundredths of a Kelvin (Figure 17, middle panels). It is noted that the inter-platform discrepancies shown here do not all agree with those obtained in studies involving the use of simultaneous nadir overpasses to perform cross-platform inter-calibration (Zou and Wang, 2011).

Results for AMSU-A channels 11, 13, and 14, which peak in the stratosphere, are presented in Figure 18. These channels are highlighted because their weighting functions peak at approximately the same levels as SSU channels 1-3 (Figure 16), although it is recognized that the two instruments differ fundamentally in that SSU measures in the infrared whereas AMSU-A measures in the microwave. The comparison is of interest nonetheless considering that the weighting functions for AMSU-A (SSU) channels 11 (1), 13 (2), and 14 (3) peak at 24 (13), 5 (4), and 2 (1) hPa. Note that AMSU-A channel 11 is chosen instead of channel 12, which has a weighting function that peaks at 11 hPa, in order to provide a more appropriate comparison with SSU channel 1, which has a skewed weighting function whose tail extends into the lower stratosphere.

The observed brightness temperatures for channel 11 (Fig. 18, upper-left, top) indicate that NOAA-15 and NOAA-16 observations are ~1.0 K warmer than those from NOAA-17 and later satellites. This is consistent with the tropospheric channels shown in Figure 17. The bias correction for this channel (Fig. 18, upper-left, bottom) accounts for this difference, and the mean background departures are consistent to within hundredths of a Kelvin (Fig 18, upper-left, middle).

NOAA-16 channel 13 is seen to be an outlier in mean brightness temperature (Fig. 18, upper-right, top), and the mean bias correction for NOAA-15 changes by -0.5K with the introduction of NOAA-16 in November 2000. When NOAA-16 is disabled in January 2005, the bias correction of NOAA-15 and Aqua changes by 0.5K. While not as large in magnitude, the background departures (Fig. 18, upper-right, middle) for this channel show corresponding adjustments. The

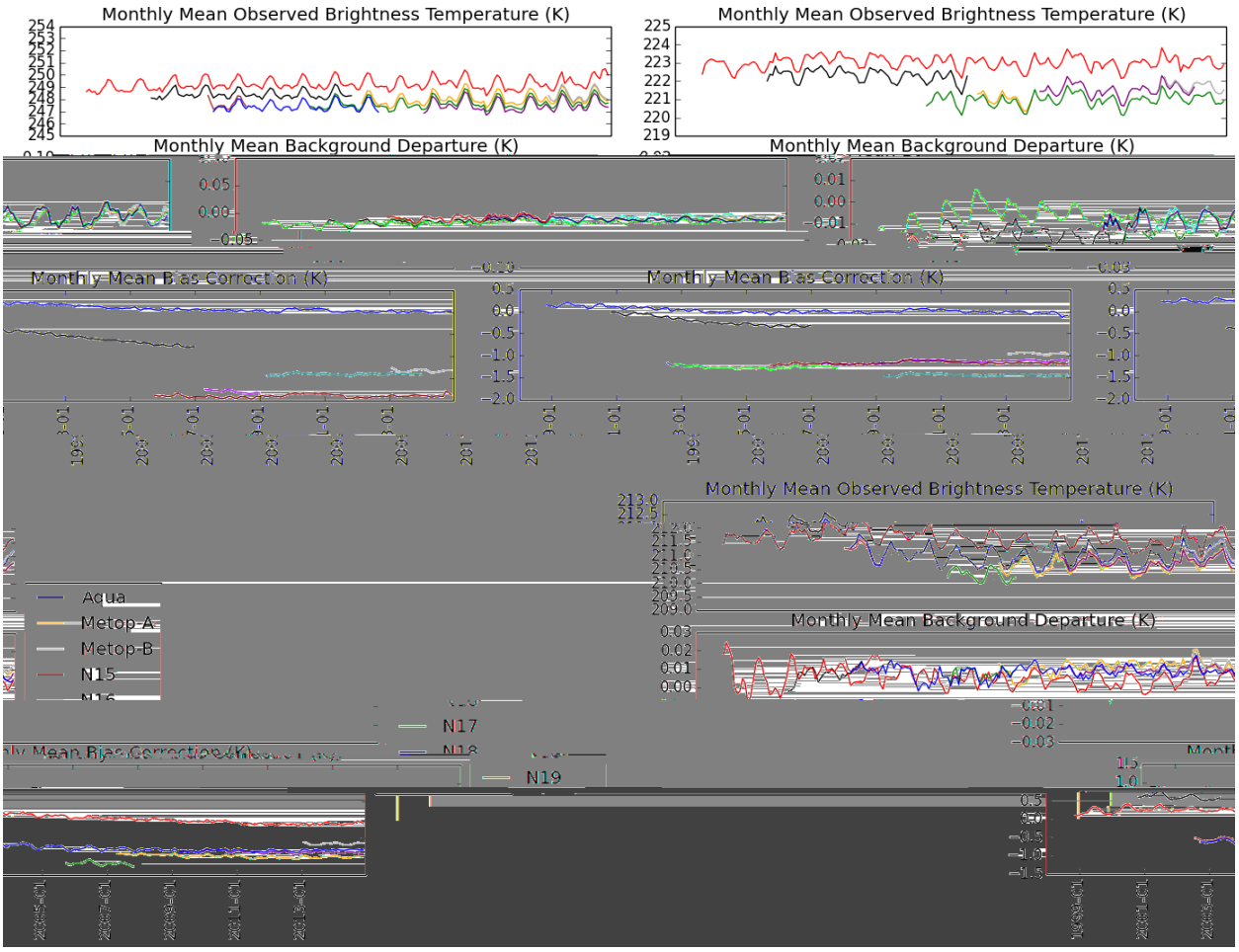

Figure 17 - Same as Figure 15, but for Advanced Microwave Sounding Unit-A Channel 5 (upper-left), Channel 7 (upper-right), and Channel 9 (lower-left).

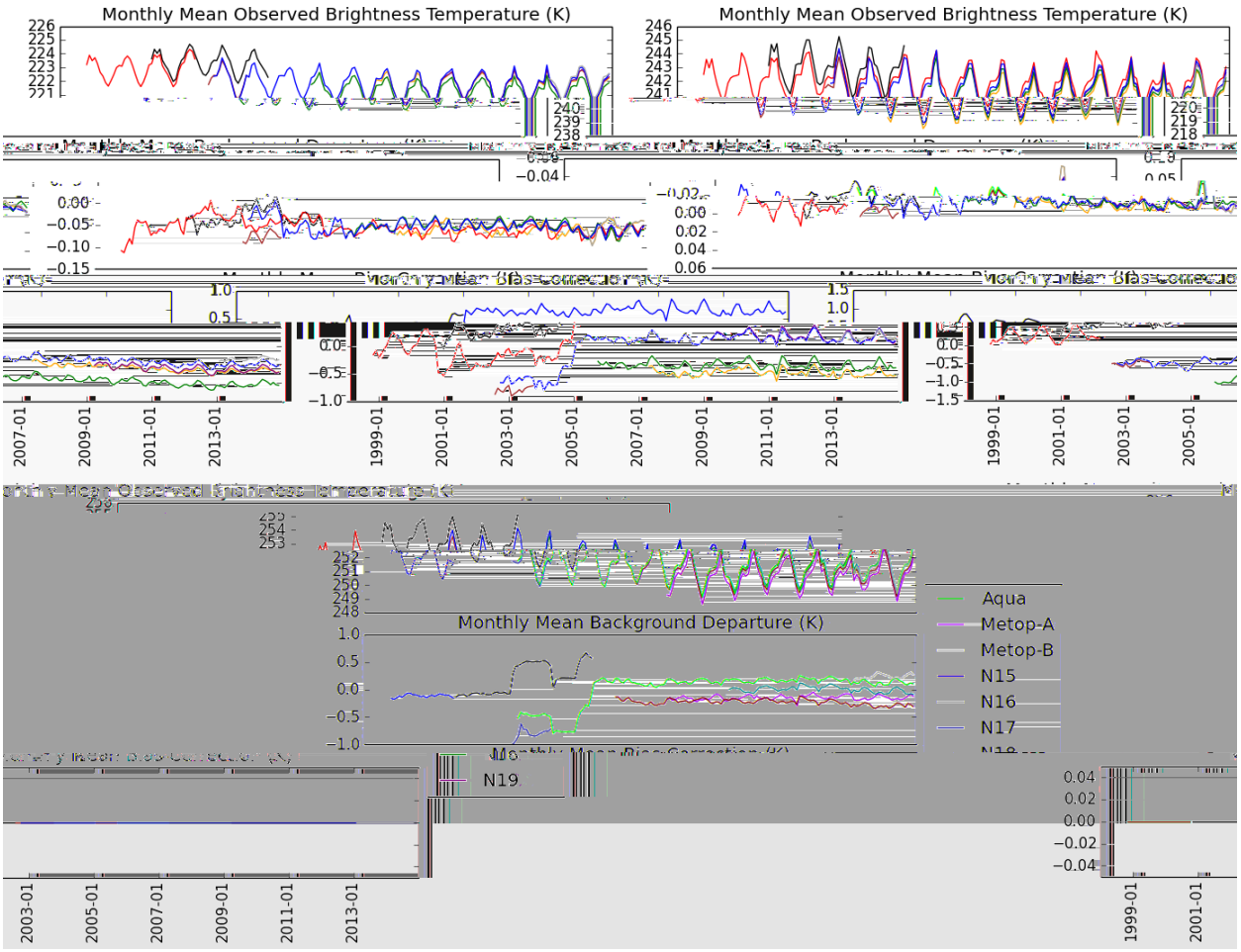

Figure 18 - Same as Figure 15, but for Advanced Microwave Sounding Unit-A Channel 11 (upper-left), Channel 13 (upper-right), and Channel 14 (lower-left).

background departures for channel 14, to which no bias correction is applied (Fig. 18, lower-left, bottom), show similar jumps with the introduction of these new platforms (Fig. 18, lower-left, middle). After the introduction of MLS temperature observations in Aug 2004 (Fig. 2), the behavior of these high-peaking channels becomes more stable and less sensitive to the introduction of new platforms. Finally, note that for channel 14, inter-platform comparisons between NOAA-15 and NOAA-16 are precluded by the failure of this channel on NOAA-15 on 30 Oct 2000, and the fact that NOAA-16 data were unavailable prior to 5 Nov 2000.

3.8 Special Sensor Microwave/Imager (SSM/I) Radiances

Radiances from the Special Sensor Microwave/Imager (SSM/I) provide the primary source of global water vapor information over the oceans from July 1987 until the introduction of the Advanced Microwave Sounding Unit-B (AMSU-B) in November 1998. The data record begins with DMSP F08 and continues on DMSP F10, F11, F13, F14, and F15. The data were active in MERRA-2 through 4 Nov 2009, when the instrument on F13 failed. The use of SSM/I in MERRA-2 differs from that in MERRA in that changes to both the thinning mesh and gross error checks result in a 90% increase in the number of assimilated observations. Note also that MERRA-2 uses the newer RSS Version 7 recalibrated radiances (Wentz 2013), whereas MERRA used RSS Version 6. Preliminary testing for MERRA-2 showed a marked difference in performance and model response to these two recalibrated datasets.

The mean background departures for SSM/I channel 3 at 22 GHz (Figure 19, middle) exhibit a marked shift for all instruments beginning in Sept 2002, which appears unaccounted for by the variational bias correction scheme (Fig. 19, bottom). Additional experimentation has confirmed that this shift occurs in conjunction with the introduction of AIRS observations in MERRA-2, although further investigation is required to determine the impact of these observations on the gridded reanalysis fields. With the exception of channels 6 and 7 on F08, which degrade over time, the SSM/I record for all other channels (not shown) has an inter-platform consistency comparable to that of channel 3 in Figure 19.

3.9 Ozone Retrievals

Figure 6a shows the time series of the globally averaged (not area-weighted) monthly mean background and analysis departures for total ozone observations. Also shown are the monthly data counts (Figure 6b) and the latitudinal extent of the observations as a function of time (Figure 6c). The SBUV background departures range between ~0 DU and 3.5 DU, with the lowest values occurring during periods when data from more than one instrument are assimilated. Most of the departure values are positive, indicating that the model-produced global total ozone is biased relative to SBUV observations, although the bias is small compared to typical global total ozone values of about 300 DU. The analysis departures, which are a measure of the closeness of the MERRA-2 analysis to observations, are consistently about 1 DU (~0.3 %) for SBUV and essentially zero during the EOS Aura period, indicating very good performance of the assimilation system. An improved agreement with data following the introduction of EOS Aura observations is clearly seen. Note that the number of assimilated OMI observations is an order of magnitude larger than that of total column SBUV. Orbital drifts of the NOAA-11 and NOAA-14 satellites

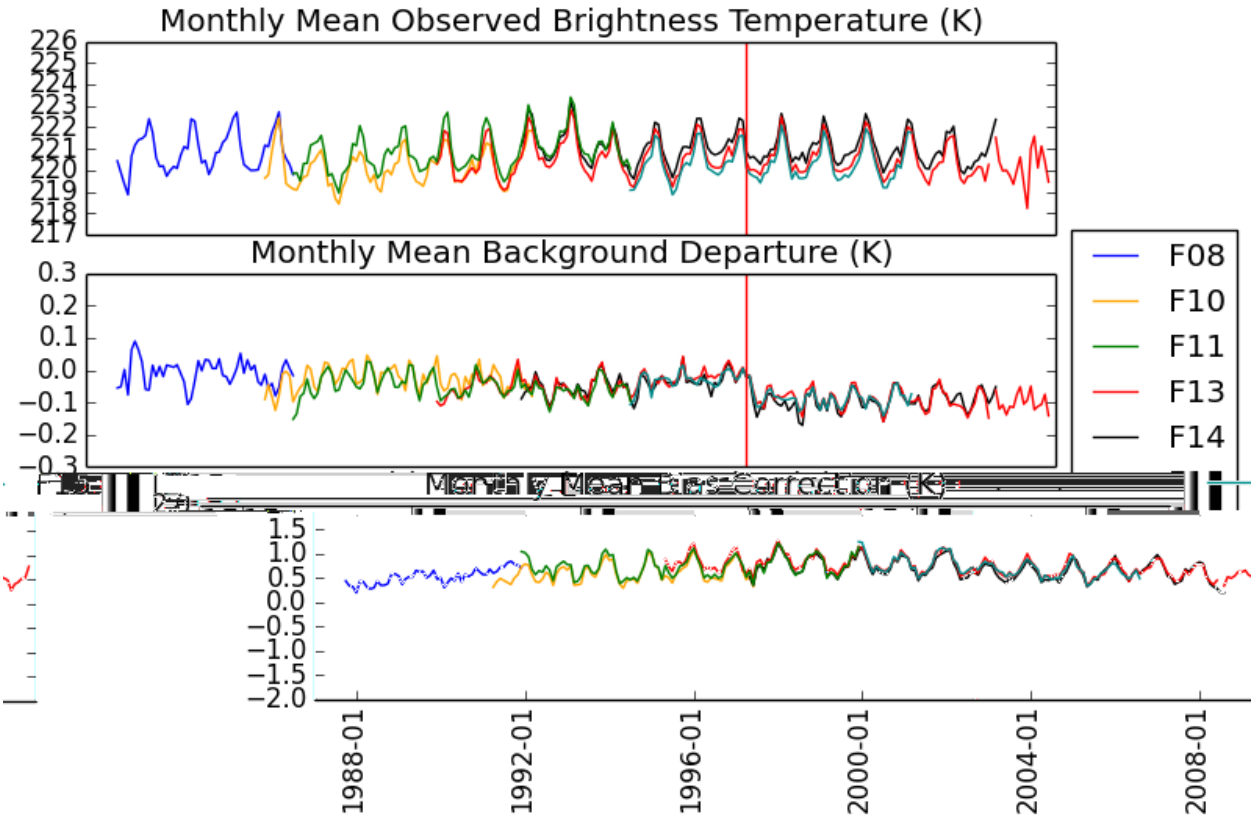

Figure 19 - SSM/I channel 3 monthly mean observed brightness temperatures (top), bias corrected background departure (middle), and bias correction (bottom). The vertical red line corresponds to the onset of AIRS observations in Sept 2002.

result in reduced coverage in 1994 and 2001. During those periods the quality of the ozone analysis at middle and high latitudes in MERRA-2 is degraded, especially during the second half of 1994.

In summary, the global total ozone in MERRA-2 exhibits a close fit to the assimilated data throughout the entire period of reanalysis. The data coverage is almost complete in the sunlit atmosphere, except in 1994 and 2001. In addition, ozone in the stratosphere is well constrained between 82°S and 82°N in all seasons by MLS observations from October 2004 onward.

4. Summary

This document summarizes the input observations into the MERRA-2 reanalysis and provides an overview of the behavior of the reanalysis in the context of these inputs. It is intended to provide a complete documentation of the input datasets, though certain specifics (e.g. individual channel failures, data drop outs) are not explicitly discussed. That said, the overall methods and rationale used to assimilate the full global observing system, both in terms of terrestrial and spaceborne observations, are presented. Future reanalyses will explicitly leverage, and improve upon, the observations presented in this document.

The observation feedback assessments are performed at the datum-level, but these data will not be publicly released as part of MERRA-2. The feedbacks are being aggregated to gridded summaries, though these summaries have also not yet been released as part of the MERRA-2 suite as of this writing. The inclusion of these feedbacks at the datum-level is under consideration for future reanalyses at the GMAO as well as at other international reanalysis centers.

MERRA-2 successfully utilizes the global observing system over the modern era, exploiting the information content contained therein to the fullest extent of the system's capability. Further evaluation is constantly underway by both internal developers and external users. There are active efforts at the GMAO focused not only on improving the data assimilation system but also on improving and advancing the underlying observations. This includes extensions to upcoming new observations, the inclusion of previously unused historical observations, and the use of advanced/reprocessed historical observations. This document aims to serve not only as public documentation of the current product but also as a baseline for the observing system used in future GMAO-generated reanalyses.

Acknowledgements

We'd like to thank Rob Lucchesi, Larry Takacs, Andrea Molod, Mike Bosilovich, Michele Rienecker, Steve Bloom, Austin Conaty, Ricardo Todling, and Steven Pawson, all of whom contributed in the development, analysis, and assembly of the MERRA-2 system and its observations. This product was supported by NASA's Modeling, Analysis, and Prediction program, and computing resources were made available by the NASA Center for Climate Simulation.

References

Bormann, N., A. J. Geer, and S. J. English, 2012: Evaluation of the microwave ocean surface emissivity model FASTEM-5 in the IFS. ECMWF Technical Memorandum 667, 18 pp.

Bosilovich, M. G., and Coauthors, 2015: MERRA-2: Initial Evaluation of the Climate. Technical Report Series on Global Modeling and Data Assimilation 43, 139 pp.

Buchard, V., and Coauthors, 2016: The MERRA-2 Aerosol Reanalysis, 1980–onward, Part 2: Data Assimilation. Journal of Climate, submitted.

Chen, Y., F. Weng, Y. Han, and Q. Liu, 2008: Validation of the Community Radiative Transfer Model by using CloudSat data. J. Geophys. Res., 113, D00A03. doi: 10.1029/2007jd009561

Chen, Y., Y. Han, Q. Liu, P. V. Delst, and F. Weng, 2011: Community Radiative Transfer Model for Stratospheric Sounding Unit. Journal of Atmospheric and Oceanic Technology, 28, 767-778. doi: 10.1175/2010JTECHA1509.1

Chen, Y., Y. Han, and F. Weng, 2012: Comparison of two transmittance algorithms in the community radiative transfer model: Application to AVHRR. J. Geophys. Res., 117, D06206. doi: 10.1029/2011jd016656

Cucurull, L., J. C. Derber, and R. J. Purser, 2013: A bending angle forward operator for global positioning system radio occultation measurements. Journal of Geophysical Research: Atmospheres, 118, 14-28. doi: 10.1029/2012JD017782

Dee, D. P., and S. M. Uppala, 2008: Variational bias correction in ERA-Interim. ECMWF Technical Memorandum 575, 26 pp.

Derber, J. C., and W.-S. Wu, 1998: The Use of TOVS Cloud-Cleared Radiances in the NCEP SSI Analysis System. Monthly Weather Review, 126, 2287-2299. doi: 10.1175/1520-0493(1998)126<2287:tuotcc>2.0.co;2

Dworak, R., and J. R. Key, 2009: Twenty Years of Polar Winds from AVHRR: Validation and Comparison with ERA-40. Journal of Applied Meteorology and Climatology, 48, 24-40. doi: 10.1175/2008JAMC1863.1

Frith, S. M., N. A. Kramarova, R. S. Stolarski, R. D. McPeters, P. K. Bhartia, and G. J. Labow, 2014: Recent changes in total column ozone based on the SBUV Version 8.6 Merged Ozone Data Set. Journal of Geophysical Research: Atmospheres, 119, 9735-9751. doi: 10.1002/2014JD021889

Gelaro, R., and Coauthors, 2016: The Modern-Era Retrospective Analysis for Research and Applications, Version-2 (MERRA-2). Journal of Climate, submitted.

Han, Y., P. van Delst, Q. Liu, F. Weng, B. Yan, R. Treadon, and J. Derber, 2006: Community Radiative Transfer Model (CRTM): Version 1. NOAA Technical Report NESDIS 122, 122 pp.

Healy, S., 2008: Assimilation of GPS radio occultation measurements at ECMWF. Proceedings of the GRAS SAF Workshop on Applications of GPSRO measurements, ECMWF, Reading, UK, 99-109.

Key, J. R., and Coauthors, 2003: Cloud-drift and water vapor winds in the polar regions from MODIS. IEEE Transactions on Geoscience and Remote Sensing, 41, 482-492. doi: 10.1109/TGRS.2002.808238

Kleist, D. T., D. F. Parrish, J. C. Derber, R. Treadon, W.-S. Wu, and S. Lord, 2009: Introduction of the GSI into the NCEP Global Data Assimilation System. Weather and Forecasting, 24, 1691-1705. doi: 10.1175/2009WAF2222201.1

Kummerow, C., and Coauthors, 2001: The Evolution of the Goddard Profiling Algorithm (GPROF) for Rainfall Estimation from Passive Microwave Sensors. Journal of Applied Meteorology, 40, 1801-1820. doi: 10.1175/1520-0450(2001)040<1801:TEOTGP>2.0.CO;2

Levelt, P. F., and Coauthors, 2006: The ozone monitoring instrument. IEEE Transactions on Geoscience and Remote Sensing, 44, 1093-1101. doi: 10.1109/TGRS.2006.872333

Liu, Q., T. Marchok, H.-L. Pan, M. Bender, and S. Lord, 2000: Improvements in Hurricane Initialization and Forecasting at NCEP with Global and Regional (GFDL) models. NWS Tech Report 472, 7 pp.

Liu, Q., F. Weng, and S. J. English, 2011: An Improved Fast Microwave Water Emissivity Model. Geoscience and Remote Sensing, IEEE Transactions on, 49, 1238-1250. doi: 10.1109/tgrs.2010.2064779

Livesey, N. J., and Coauthors, 2013a: Earth Observing System Aura Microwave Limb Sounder Version 3.3 and 3.4 Level 2 Data Quality and Description Document. Jet Propulsion Laboratory Technical Memo D-33509, 158 pp.

Livesey, N. J., and Coauthors, 2013b: Earth Observing System Aura Microwave Limb Sounder Version 2.2 and 2.3 Level 2 Data Quality and Description Document. Jet Propulsion Laboratory Technical Memo D-33509, 110 pp.

Livesey, N. J., and Coauthors, 2016: Earth Observing System Aura Microwave Limb Sounder Version 4.2x Level 2 Data Quality and Description Document. Jet Propulsion Laboratory Technical Memo D-33509 Rev. B, 164 pp.

McPeters, R. D., P. K. Bhartia, D. Haffner, G. J. Labow, and L. Flynn, 2013: The version 8.6 SBUV ozone data record: An overview. Journal of Geophysical Research: Atmospheres, 118, 8032-8039. doi: 10.1002/jgrd.50597

Molod, A., L. Takacs, M. Suarez, and J. Bacmeister, 2015: Development of the GEOS-5 atmospheric general circulation model: evolution from MERRA to MERRA2. Geosci. Model Dev., 8, 1339-1356. doi: 10.5194/gmd-8-1339-2015

Nalli, N. R., P. J. Minnett, E. Maddy, W. W. McMillan, and M. D. Goldberg, 2008a: Emissivity and reflection model for calculating unpolarized isotropic water surface-leaving radiance in

the infrared. 2: Validation using Fourier transform spectrometers. Applied optics, 47, 4649-4671.

Nalli, N. R., P. J. Minnett, and P. Van Delst, 2008b: Emissivity and reflection model for calculating unpolarized isotropic water surface-leaving radiance in the infrared. I: Theoretical development and calculations. Applied optics, 47, 3701-3721.

Nieman, S. J., W. P. Menzel, C. M. Hayden, D. Gray, S. T. Wanzong, C. S. Velden, and J. Daniels, 1997: Fully Automated Cloud-Drift Winds in NESDIS Operations. Bulletin of the American Meteorological Society, 78, 1121-1133. doi: 10.1175/1520-0477(1997)078<1121:FACDWI>2.0.CO;2

Olson, W. S., and Coauthors, 2006: Precipitation and Latent Heating Distributions from Satellite Passive Microwave Radiometry. Part I: Improved Method and Uncertainties. Journal of Applied Meteorology and Climatology, 45, 702-720. doi: 10.1175/JAM2369.1

Randles, C. A., and Coauthors, 2016a: The MERRA-2 Aerosol Reanalysis, 1980–onward, Part 1: System Description and Data Assimilation Evaluation. Journal of Climate, submitted.

Randles, C. A., and Coauthors, 2016b: The MERRA-2 Aerosol Assimilation. Technical Report Series on Global Modeling and Data Assimilation 45, 132 pp.

Rienecker, M. M., and Coauthors, 2008: The GEOS-5 Data Assimilation System—Documentation of Versions 5.0.1, 5.1.0, and 5.2.0. Technical Report Series on Global Modeling and Data Assimilation 27, 109 pp.

Rienecker, M. M., and Coauthors, 2011: MERRA: NASA's Modern-Era Retrospective Analysis for Research and Applications. Journal of Climate, 24, 3624-3648. doi: 10.1175/jcli-d-11-00015.1

Schwartz, M. J., and Coauthors, 2008: Validation of the Aura Microwave Limb Sounder temperature and geopotential height measurements. Journal of Geophysical Research: Atmospheres, 113, D15S11. doi: 10.1029/2007JD008783

Takacs, L., M. Suarez, and R. Todling, 2014: Maintaining Atmospheric Mass and Water Balance Within Reanalysis. Technical Report Series on Global Modeling and Data Assimilation 37, 39 pp.

Treadon, R. E., H.-L. Pan, W.-S. Wu, Y. Lin, W. S. Olson, and R. J. Kuligowski, 2002: Global and Regional Moisture Analyses at NCEP. Proc. ECMWF/GEWEX Workshop on Humidity Analysis, Reading, UK, 33-47.

Velden, C. S., C. M. Hayden, S. J. Nieman, W. P. Menzel, S. Wanzong, and J. S. Goerss, 1997: Upper-Tropospheric Winds Derived from Geostationary Satellite Water Vapor Observations. Bulletin of the American Meteorological Society, 78, 173-195. doi: 10.1175/1520-0477(1997)078<0173:UTWDFG>2.0.CO;2

Wargan, K., and Coauthors, 2015: The global structure of upper troposphere-lower stratosphere ozone in GEOS-5: A multiyear assimilation of EOS Aura data. Journal of Geophysical Research: Atmospheres, 120, 2013-2036. doi: 10.1002/2014JD022493

Waters, J. W., and Coauthors, 2006: The Earth observing system microwave limb sounder (EOS MLS) on the aura Satellite. IEEE Transactions on Geoscience and Remote Sensing, 44, 1075-1092. doi: 10.1109/TGRS.2006.873771

Wentz, F. J., 2013: SSM/I Version-7 Calibration Report. Remote Sensing Systems Technical Report 011012, 46 pp.

Wu, W.-S., R. J. Purser, and D. F. Parrish, 2002: Three-Dimensional Variational Analysis with Spatially Inhomogeneous Covariances. Monthly Weather Review, 130, 2905-2916.

Yang, R., A. D. Collard, J. Derber, and Y.-T. Hou, 2012: Temporal and Spatial Variation of Trace Gases and Their Impact on Satellite Radiance Data Assimilation. 4th WCRP International Conference on Reanalysis, Silver Spring, MD.

Yang, S., W. S. Olson, J.-J. Wang, T. L. Bell, E. A. Smith, and C. D. Kummerow, 2006: Precipitation and Latent Heating Distributions from Satellite Passive Microwave Radiometry. Part II: Evaluation of Estimates Using Independent Data. Journal of Applied Meteorology and Climatology, 45, 721-739. doi: 10.1175/JAM2370.1

Zou, C.-Z., M. D. Goldberg, Z. Cheng, N. C. Grody, J. T. Sullivan, C. Cao, and D. Tarpley, 2006: Recalibration of microwave sounding unit for climate studies using simultaneous nadir overpasses. Journal of Geophysical Research: Atmospheres, 111, D19114. doi: 10.1029/2005JD006798

Zou, C.-Z., and W. Wang, 2010: Stability of the MSU-Derived Atmospheric Temperature Trend. Journal of Atmospheric and Oceanic Technology, 27, 1960-1971. doi: 10.1175/2009JTECHA1333.1

Appendix A – Channel Selection for AIRS, IASI, and CrIS

Channel Selection for Hyperspectral Instruments											
AIRS				IASI				CrIS			
Subset #	Instrument #	Wavenumber (cm-1)	Wavelength (μm)	Subset #	Instrument #	Wavenumber (cm-1)	Wavelength (μm)	Subset #	Instrument #	Wavenumber (cm-1)	Wavelength (μm)
3	7	651.05	15.360	1	16	648.75	15.414	1	27	666.25	15.009
6	15	652.97	15.315	5	38	654.25	15.285	23	83	701.25	14.260
9	20	654.18	15.286	9	49	657.00	15.221	26	88	704.38	14.197
10	21	654.42	15.281	11	51	657.50	15.209	27	89	705.00	14.184
11	22	654.66	15.275	13	55	658.50	15.186	29	95	708.75	14.109
13	27	655.87	15.247	15	57	659.00	15.175	30	96	709.38	14.097
14	28	656.12	15.241	16	59	659.50	15.163	31	99	711.25	14.060
18	40	659.05	15.173	17	61	660.00	15.152	32	101	712.50	14.035
21	52	662.02	15.105	19	63	660.50	15.140	33	102	713.13	14.023
29	69	666.26	15.009	20	66	661.25	15.123	34	104	714.38	13.998
31	72	667.02	14.992	22	70	662.25	15.100	35	106	715.63	13.974
44	92	672.10	14.879	23	72	662.75	15.089	36	107	716.25	13.962
45	93	672.36	14.873	24	74	663.25	15.077	39	116	721.88	13.853
46	98	673.64	14.845	27	79	664.50	15.049	40	120	724.38	13.805
47	99	673.90	14.839	28	81	665.00	15.038	41	123	726.25	13.769
49	104	675.19	14.811	30	83	665.50	15.026	42	124	726.88	13.758
50	105	675.45	14.805	32	85	666.00	15.015	43	125	727.50	13.746
52	110	676.75	14.777	34	87	666.50	15.004	44	126	728.13	13.734
53	111	677.01	14.771	43	104	670.75	14.909	45	130	730.63	13.687
55	116	678.31	14.743	44	106	671.25	14.898	46	132	731.88	13.664
56	117	678.57	14.737	45	109	672.00	14.881	47	133	732.50	13.652

57	123	680.14	14.703	47	111	672.50	14.870	48	136	734.38	13.617
59	128	681.46	14.674	48	113	673.00	14.859	49	137	735.00	13.605
60	129	681.72	14.669	49	116	673.75	14.842	50	138	735.63	13.594
61	138	689.49	14.503	50	119	674.50	14.826	51	142	738.13	13.548
62	139	689.76	14.498	51	122	675.25	14.809	52	143	738.75	13.536
63	144	691.12	14.469	52	125	676.00	14.793	53	144	739.38	13.525
64	145	691.39	14.464	53	128	676.75	14.777	54	145	740.00	13.514
65	150	692.76	14.435	54	131	677.50	14.760	57	150	743.13	13.457
66	151	693.03	14.429	55	133	678.00	14.749	58	151	743.75	13.445
67	156	694.40	14.401	56	135	678.50	14.738	59	153	745.00	13.423
68	157	694.67	14.395	57	138	679.25	14.722	60	154	745.63	13.412
70	162	696.05	14.367	58	141	680.00	14.706	61	155	746.25	13.400
72	168	697.71	14.333	59	144	680.75	14.690	62	157	747.50	13.378
73	169	697.99	14.327	60	146	681.25	14.679	63	158	748.13	13.367
75	172	698.82	14.310	61	148	681.75	14.668	64	159	748.75	13.356
76	173	699.10	14.304	63	151	682.50	14.652	65	160	749.38	13.344
77	174	699.38	14.298	64	154	683.25	14.636	66	161	750.00	13.333
78	175	699.66	14.293	65	157	684.00	14.620	67	162	750.63	13.322
80	179	700.78	14.270	66	159	684.50	14.609	68	163	751.25	13.311
81	180	701.06	14.264	68	161	685.00	14.599	69	164	751.88	13.300
83	185	702.46	14.236	69	163	685.50	14.588	70	165	752.50	13.289
84	186	702.74	14.230	70	167	686.50	14.567	71	166	753.13	13.278
85	190	703.87	14.207	71	170	687.25	14.551	72	168	754.38	13.256
86	192	704.44	14.196	72	173	688.00	14.535	73	170	755.63	13.234
87	198	706.14	14.162	73	176	688.75	14.519	74	171	756.25	13.223
88	201	706.99	14.144	75	180	689.75	14.498	75	173	757.50	13.201
89	204	707.85	14.127	76	185	691.00	14.472	76	175	758.75	13.180
90	207	708.71	14.110	77	187	691.50	14.461	79	198	773.13	12.935
91	210	709.57	14.093	79	193	693.00	14.430	80	208	779.38	12.831
92	215	711.01	14.065	81	199	694.50	14.399	81	211	781.25	12.800

93	216	711.29	14.059	85	205	696.00	14.368	82	216	784.38	12.749
94	221	712.74	14.030	86	207	696.50	14.358	83	224	789.38	12.668
95	226	714.19	14.002	87	210	697.25	14.342	84	228	791.88	12.628
96	227	714.48	13.996	88	212	697.75	14.332	85	236	796.88	12.549
97	232	715.94	13.968	90	214	698.25	14.322	86	238	798.13	12.529
98	252	721.84	13.854	91	217	699.00	14.306	87	242	800.63	12.490
99	253	722.14	13.848	93	219	699.50	14.296	88	248	804.38	12.432
100	256	723.03	13.831	94	222	700.25	14.281	89	266	815.63	12.261
101	257	723.33	13.825	95	224	700.75	14.270	90	268	816.88	12.242
102	261	724.52	13.802	97	226	701.25	14.260	91	279	823.75	12.140
103	262	724.82	13.796	99	230	702.25	14.240	92	283	826.25	12.103
104	267	726.33	13.768	101	232	702.75	14.230	93	311	843.75	11.852
105	272	727.83	13.739	102	236	703.75	14.210	101	342	863.13	11.586
106	295	734.15	13.621	104	239	704.50	14.194	113	392	894.38	11.181
107	299	735.38	13.598	105	243	705.50	14.174	120	404	901.88	11.088
109	305	737.24	13.564	106	246	706.25	14.159	121	427	916.25	10.914
110	310	738.79	13.536	107	249	707.00	14.144	122	447	928.75	10.767
113	333	746.01	13.405	108	252	707.75	14.129	123	464	939.38	10.645
114	338	747.60	13.376	109	254	708.25	14.119	124	473	945.00	10.582
115	355	753.06	13.279	111	260	709.75	14.089	125	482	950.63	10.519
116	362	755.33	13.239	112	262	710.25	14.080	126	484	951.88	10.506
117	375	759.57	13.165	113	265	711.00	14.065	128	529	980.00	10.204
119	475	801.10	12.483	114	267	711.50	14.055	185	716	1212.50	8.247
121	497	809.18	12.358	115	269	712.00	14.045	226	794	1310.00	7.634
122	528	820.83	12.183	116	275	713.50	14.015	228	798	1315.00	7.605
123	587	843.91	11.850	118	282	715.25	13.981	229	800	1317.50	7.590
124	672	871.29	11.477	120	294	718.25	13.923	230	802	1320.00	7.576
125	787	917.31	10.901	121	296	718.75	13.913	237	811	1331.25	7.512
126	791	918.75	10.884	122	299	719.50	13.899	239	814	1335.00	7.491
128	870	948.18	10.546	124	303	720.50	13.879	261	840	1367.50	7.313

129	914	965.43	10.358	125	306	721.25	13.865	274	854	1385.00	7.220
130	950	979.13	10.213	129	323	725.50	13.784	275	856	1387.50	7.207
166	1301	1236.54	8.087	131	327	726.50	13.765	276	861	1393.75	7.175
167	1304	1238.11	8.077	132	329	727.00	13.755	277	862	1395.00	7.168
168	1329	1251.36	7.991	134	335	728.50	13.727	278	864	1397.50	7.156
169	1371	1285.48	7.779	135	345	731.00	13.680	279	865	1398.75	7.149
170	1382	1291.71	7.742	136	347	731.50	13.671	280	866	1400.00	7.143
171	1415	1310.77	7.629	137	350	732.25	13.657	281	867	1401.25	7.136
172	1424	1316.06	7.598	138	354	733.25	13.638	282	869	1403.75	7.124
173	1449	1330.98	7.513	139	356	733.75	13.629	283	871	1406.25	7.111
174	1455	1334.61	7.493	140	360	734.75	13.610	284	872	1407.50	7.105
176	1477	1345.31	7.433	142	366	736.25	13.582	285	874	1410.00	7.092
177	1500	1357.24	7.368	143	371	737.50	13.559	286	876	1412.50	7.080
178	1519	1367.25	7.314	145	373	738.00	13.550	287	878	1415.00	7.067
181	1565	1392.15	7.183	146	375	738.50	13.541	288	879	1416.25	7.061
182	1574	1397.14	7.158	147	377	739.00	13.532	289	880	1417.50	7.055
186	1627	1427.23	7.007	148	379	739.50	13.523	290	884	1422.50	7.030
190	1669	1468.83	6.808	149	381	740.00	13.514	291	886	1425.00	7.018
193	1694	1484.37	6.737	150	383	740.50	13.504	292	887	1426.25	7.011
202	1766	1544.48	6.475	151	386	741.25	13.491	293	888	1427.50	7.005
208	1800	1567.89	6.378	152	389	742.00	13.477	294	889	1428.75	6.999
212	1826	1586.26	6.304	153	398	744.25	13.436	295	890	1430.00	6.993
215	1865	2181.50	4.584	154	401	745.00	13.423	296	900	1442.50	6.932
216	1866	2182.40	4.582	155	404	745.75	13.409	297	921	1468.75	6.809
217	1868	2184.21	4.578	157	407	746.50	13.396	298	924	1472.50	6.791
218	1869	2185.12	4.576	159	410	747.25	13.382	299	927	1476.25	6.774
219	1872	2187.85	4.571	161	414	748.25	13.365	300	945	1498.75	6.672
220	1873	2188.76	4.569	162	416	748.75	13.356	301	991	1556.25	6.426
221	1876	2191.50	4.563	165	426	751.25	13.311	302	994	1560.00	6.410
222	1881	2196.08	4.554	166	428	751.75	13.302	303	1007	1576.25	6.344

223	1882	2196.99	4.552		167	432	752.75	13.285		304	1015	1586.25	6.304
225	1911	2223.94	4.497		169	434	753.25	13.276		305	1030	1605.00	6.231
226	1917	2229.59	4.485		170	439	754.50	13.254		306	1094	1685.00	5.935
227	1918	2230.54	4.483		172	445	756.00	13.228		307	1106	1700.00	5.882
228	1924	2236.23	4.472		174	457	759.00	13.175		308	1130	1730.00	5.780
229	1928	2240.03	4.464		180	515	773.50	12.928		309	1132	1732.50	5.772
					181	546	781.25	12.800		310	1133	1733.75	5.768
					182	552	782.75	12.775		311	1135	1736.25	5.760
					183	559	784.50	12.747		312	1142	1745.00	5.731
					184	566	786.25	12.719					
					185	571	787.50	12.698					
					186	573	788.00	12.690					
					191	646	806.25	12.403					
					192	662	810.25	12.342					
					193	668	811.75	12.319					
					196	756	833.75	11.994					
					198	867	861.50	11.608					
					199	906	871.25	11.478					
					200	921	875.00	11.429					
					201	1027	901.50	11.093					
					202	1046	906.25	11.034					
					205	1121	925.00	10.811					
					206	1133	928.00	10.776					

Table 4 - Assimilated channels for AIRS, IASI, and CrIS. Shaded CrIS channels were used through 31 July 2012.

Previous Volumes in This Series

Volume 1 *September 1994*	Documentation of the Goddard Earth Observing System (GEOS) general circulation model - Version 1 **L.L. Takacs, A. Molod, and T. Wang**
Volume 2 *October 1994*	Direct solution of the implicit formulation of fourth order horizontal diffusion for gridpoint models on the sphere **Y. Li, S. Moorthi, and J.R. Bates**
Volume 3 *December 1994*	An efficient thermal infrared radiation parameterization for use in general circulation models **M.-D. Chou and M.J. Suarez**
Volume 4 *January 1995*	Documentation of the Goddard Earth Observing System (GEOS) Data Assimilation System - Version 1 **James Pfaendtner, Stephen Bloom, David Lamich, Michael Seablom, Meta Sienkiewicz, James Stobie, and Arlindo da Silva**
Volume 5 *April 1995*	Documentation of the Aries-GEOS dynamical core: Version 2 **Max J. Suarez and Lawrence L. Takacs**
Volume 6 *April 1995*	A Multiyear Assimilation with the GEOS-1 System: Overview and Results **Siegfried Schubert, Chung-Kyu Park, Chung-Yu Wu, Wayne Higgins, Yelena Kondratyeva, Andrea Molod, Lawrence Takacs, Michael Seablom, and Richard Rood**
Volume 7 *September 1995*	Proceedings of the Workshop on the GEOS-1 Five-Year Assimilation **Siegfried D. Schubert and Richard B. Rood**

Volume 8 *March 1996*	Documentation of the Tangent Linear Model and Its Adjoint of the Adiabatic Version of the NASA GEOS-1 C-Grid GCM: Version 5.2 **Weiyu Yang and I. Michael Navon**
Volume 9 *March 1996*	Energy and Water Balance Calculations in the Mosaic LSM **Randal D. Koster and Max J. Suarez**
Volume 10 *April 1996*	Dynamical Aspects of Climate Simulations Using the GEOS General Circulation Model **Lawrence L. Takacs and Max J. Suarez**
Volume 11 *May 1997*	Documentation of the Tangent Linear and Adjoint Models of the Relaxed Arakawa-Schubert Moisture Parameterization Package of the NASA GEOS-1 GCM (Version 5.2) **Weiyu Yang, I. Michael Navon, and Ricardo Todling**
Volume 12 *August 1997*	Comparison of Satellite Global Rainfall Algorithms **Alfred T.C. Chang and Long S. Chiu**
Volume 13 *December 1997*	Interannual Variability and Potential Predictability in Reanalysis Products **Wie Ming and Siegfried D. Schubert**
Volume 14 *August 1998*	A Comparison of GEOS Assimilated Data with FIFE Observations **Michael G. Bosilovich and Siegfried D. Schubert**
Volume 15 *June 1999*	A Solar Radiation Parameterization for Atmospheric Studies **Ming-Dah Chou and Max J. Suarez**

Volume 16

November 1999

Filtering Techniques on a Stretched Grid General Circulation Model

Lawrence Takacs, William Sawyer, Max J. Suarez, and Michael S. Fox-Rabinowitz

Volume 17

July 2000

Atlas of Seasonal Means Simulated by the NSIPP-1 Atmospheric GCM

Julio T. Bacmeister, Philip J. Pegion, Siegfried D. Schubert, and Max J. Suarez

Volume 18

December 2000

An Assessment of the Predictability of Northern Winter Seasonal Means with the NSIPP1 AGCM

Philip J. Pegion, Siegfried D. Schubert, and Max J. Suarez

Volume 19

July 2001

A Thermal Infrared Radiation Parameterization for Atmospheric Studies

Ming-Dah Chou, Max J. Suarez, Xin-Zhong Liang, and Michael M.-H. Yan

Volume 20

August 2001

The Climate of the FVCCM-3 Model

Yehui Chang, Siegfried D. Schubert, Shian-Jiann Lin, Sharon Nebuda, and Bo-Wen Shen

Volume 21

September 2001

Design and Implementation of a Parallel Multivariate Ensemble Kalman Filter for the Poseidon Ocean General Circulation Model

Christian L. Keppenne and Michele M. Rienecker

Volume 22

August 2002

A Coupled Ocean-Atmosphere Radiative Model for Global Ocean Biogeochemical Models

Watson W. Gregg

Volume 23

November 2002

Prospects for Improved Forecasts of Weather and Short-term Climate Variability on Subseasonal (2-Week to 2-Month) Time Scales

Siegfried D. Schubert, Randall Dole, Huang van den Dool, Max J. Suarez, and Duane Waliser

Volume 24

July 2003

Temperature Data Assimilation with Salinity Corrections: Validation for the NSIPP Ocean Data Assimilation System in the Tropical Pacific Ocean, 1993–1998

Alberto Troccoli, Michele M. Rienecker, Christian L. Keppenne, and Gregory C. Johnson

Volume 25

December 2003

Modeling, Simulation, and Forecasting of Subseasonal Variability

Duane Waliser, Siegfried D. Schubert, Arun Kumar, Klaus Weickmann, and Randall Dole

Volume 26

April 2005

Documentation and Validation of the Goddard Earth Observing System (GEOS) Data Assimilation System – Version 4

Senior Authors: S. Bloom, A. da Silva and D. Dee

Contributing Authors: M. Bosilovich, J-D. Chern, S. Pawson, S. Schubert, M. Sienkiewicz, I. Stajner, W-W. Tan, and M-L. Wu

Volume 27

December 2008

The GEOS-5 Data Assimilation System - Documentation of Versions 5.0.1, 5.1.0, and 5.2.0.

M.M. Rienecker, M.J. Suarez, R. Todling, J. Bacmeister, L. Takacs, H.-C. Liu, W. Gu, M. Sienkiewicz, R.D. Koster, R. Gelaro, I. Stajner, and J.E. Nielsen

Volume 28

April 2012

The GEOS-5 Atmospheric General Circulation Model: Mean Climate and Development from MERRA to Fortuna

Andrea Molod, Lawrence Takacs, Max Suarez, Julio Bacmeister, In-Sun Song, and Andrew Eichmann

Volume 29

June 2012

Atmospheric Reanalyses – Recent Progress and Prospects for the Future.

A Report from a Technical Workshop, April 2010

Michele M. Rienecker, Dick Dee, Jack Woollen, Gilbert P. Compo, Kazutoshi Onogi, Ron Gelaro, Michael G. Bosilovich, Arlindo da Silva, Steven Pawson, Siegfried Schubert, Max Suarez, Dale Barker, Hirotaka Kamahori, Robert Kistler, and Suranjana Saha

Volume 30

December 2012

The GEOS-iODAS: Description and Evaluation

Guillaume Vernieres, Michele M. Rienecker, Robin Kovach and Christian L. Keppenne

Volume 31

March 2013

Global Surface Ocean Carbon Estimates in a Model Forced by MERRA

Watson W. Gregg, Nancy W. Casey and Cecile S. Rousseaux

Volume 32

March 2014

Estimates of AOD Trends (2002-2012) over the World's Major Cities based on the MERRA Aerosol Reanalysis

Simon Provencal, Pavel Kishcha, Emily Elhacham, Arlindo M. da Silva, and Pinhas Alpert

Volume 33

August 2014

The Effects of Chlorophyll Assimilation on Carbon Fluxes in a Global Biogeochemical Model

Cécile S. Rousseaux and Watson W. Gregg

Volume 34

September 2014

Background Error Covariance Estimation using Information from a Single Model Trajectory with Application to Ocean Data Assimilation into the GEOS-5 Coupled Model

Christian L. Keppenne, Michele M. Rienecker, Robin M. Kovach, and Guillaume Vernieres

Volume 35 *December 2014*	Observation-Corrected Precipitation Estimates in GEOS-5 **Rolf H. Reichle and Qing Liu**
Volume 36 *March 2015*	Evaluation of the 7-km GEOS-5 Nature Run **Ronald Gelaro, William M. Putman, Steven Pawson, Clara Draper, Andrea Molod, Peter M. Norris, Lesley Ott, Nikki Prive, Oreste Reale, Deepthi Achuthavarier, Michael Bosilovich, Virginie Buchard, Winston Chao, Lawrence Coy, Richard Cullather, Arlindo da Silva, Anton Darmenov, Ronald M. Errico, Marangelly Fuentes, Min-Jeong Kim, Randal Koster, Will McCarty, Jyothi Nattala, Gary Partyka, Siegfried Schubert, Guillaume Vernieres, Yuri Vikhliaev, and Krzysztof Wargan**
Volume 37 *March 2015*	Maintaining Atmospheric Mass and Water Balance within Reanalysis **Lawrence L. Takacs, Max Suarez, and Ricardo Todling**
Volume 38 *September 2015*	The Quick Fire Emissions Dataset (QFED) – Documentation of versions 2.1, 2.2 and 2.4 **Anton S. Darmenov and Arlindo da Silva**
Volume 39 *September 2015*	Land Boundary Conditions for the Goddard Earth Observing System Model Version 5 (GEOS-5) Climate Modeling System - Recent Updates and Data File Descriptions **Sarith Mahanama, Randal Koster, Gregory Walker, Lawrence Takacs**, **Rolf Reichle, Gabrielle De Lannoy, Qing Liu, Bin Zhao, and** Max **Suarez**
Volume 40 *October 2015*	Soil Moisture Active Passive (SMAP) Project Assessment Report for the Beta-Release L4_SM Data Product **Rolf H. Reichle, Gabrielle J. M. De Lannoy, Qing Liu, Andreas Colliander**, **Austin Conaty, Thomas Jackson, John Kimball, and Randal D. Koster**

Volume 41 *October 2015*	GDIS Workshop Report **Siegfried Schubert, Will Pozzi, Kingtse Mo, Eric Wood, Kerstin Stahl, Mike Hayes, Juergen Vogt, Sonia Seneviratne, Ron Stewart, Roger Pulwarty, and Robert Stefanski**
Volume 42 *November 2015*	Soil Moisture Active Passive (SMAP) Project Calibration and Validation for the L4_C Beta-Release Data Product **John Kimball, Lucas Jones, Joseph Glassy, E. Natasha Stavros, Nima Madani, Rolf Reichle, Thomas Jackson, and Andreas Colliander**
Volume 43 *September 2015*	MERRA-2: Initial Evaluation of the Climate **Michael G. Bosilovich, Santha Akella, Lawrence Coy, Richard Cullather, Clara Draper, Ronald Gelaro, Robin Kovach, Qing Liu, Andrea Molod, Peter Norris, Krzysztof Wargan, Winston Chao, Rolf Reichle, Lawrence Takacs, Yury Vikhliaev, Steve Bloom, Allison Collow, Stacey Firth, Gordon Labow, Gary Partyka, Steven Pawson, Oreste Reale, Siegfried Schuber**t, **and Max Suarez**
Volume 44 *February 2016*	Estimation of the Ocean Skin Temperature using the NASA GEOS Atmospheric Data Assimilation System **Santha Akella, Ricardo Todling, Max Suarez**
Volume 45 *October 2016*	The MERRA-2 Aerosol Assimilation **C. A. Randles, A. M. da Silva, V. Buchard, A. Darmenov, P. R. Colarco, V. Aquila, H. Bian, E. P. Nowottnick, X. Pan, A. Smirnov, H. Yu, and R. Govindaraju**